Available online at www.sciencedirect.com
SCIENCE DIRECT
Journal of Asian Earth Sciences 27 (2006) 717–734
Journal of Asian Earth Sciences
www.elsevier.com/locate/jaes

The Chako antiform: A folded segment of the Greater Himalayan sequence, Nar valley, Central Nepal Himalaya

Thomas P. Gleeson [a,b], Laurent Godin [c,*]

[a] Department of Earth Sciences, Simon Fraser University, 8888 University Drive, Burnaby, BC, Canada V5A1S6
[b] Department of Civil Engineering, Queen's University, Kingston, Ont., Canada K7L 3N6
[c] Department of Geological Sciences and Geological Engineering, Miller Hall, Queen's University, Kingston, Ont., Canada K7L 3N6

Received 4 January 2005; accepted 13 June 2005

Abstract

Recent and previously published mapping in the Nar valley, north of the Annapurna massif in central Nepal, recognised an enigmatic metamorphic culmination of the Greater Himalayan sequence, surrounded by rocks correlated with the Tethyan sedimentary sequence. The map area is re-interpreted as two structural levels within the Greater Himalayan sequence. The Lower Level is correlated to the well-studied Greater Himalayan sequence of the Annapurna region, based on characteristic rock types, high-strain zones with south-verging shear-sense indicators, and high-grade metamorphism. The rocks of the Upper Level, previously mapped as the sub-greenschist or zeolite facies Tethyan sedimentary sequence, are garnet-bearing schists. Petrography and garnet-biotite thermometry suggest the Upper Level equilibrated at amphibolite facies (500–650 °C). These results support the recent contention that the Upper Level rocks are a component of the Greater Himalayan sequence, and thus indicate that components of the Himalayan metamorphic core vary considerably along strike. Structural, metamorphic and age constraints are integrated into a cohesive regional tectonometamorphic model. The Lower and Upper Levels both experienced D_1 deformation and peak metamorphism before ~20 Ma. The Lower and Upper Levels were juxtaposed along the synmetamorphic Chame detachment after 20 Ma during retrograde metamorphism. After ~19 Ma, the Phu detachment placed the unmetamorphosed Tethyan sedimentary sequence above the Lower and Upper Levels. The entire package was then subsequently folded, after 19 Ma, by a non-cylindrical antiform-synform pair with a ~25 km wavelength creating an apparent dome. The proposed tectonometamorphic model reconciles previously contradictory interpretations of the transition between metamorphic core and overlying sediments in the Nar valley.

Keywords: Himalaya; Tectonics; Detachment faults; Metamorphic belts

1. Introduction

Orogenic models emanating from the well-studied Himalayan collisional system impact our understanding of older collisional orogens, exhumation of metamorphic rocks, crust and mantle dynamics, and the role of erosion and climate in mountain-building (Molnar et al., 1993; Nelson et al., 1996; Royden et al., 1997; Beaumont et al., 2001). Recent empirical and numerical models suggest the metamorphic core of the Himalayan orogen is the leading edge of a middle crustal zone originating below Tibet, which extruded southward in the Miocene (Grujic et al., 1996; Royden et al., 1997; Beaumont et al., 2001; Vannay and Grasemann, 2001; Grujic et al., 2002). The recent resurgence in detailed field studies at critical contacts and transition zones provide crucial information for orogenic models (Grujic et al., 2002; Searle et al., 2003; Law et al., 2004).

The metamorphic core of the Himalayan orogen, the Greater Himalayan sequence, is an amphibolite-facies lithotectonic unit characterised by an early schistosity overprinted by non-coaxial, south-verging high strain zones (Fig. 1; Pêcher, 1975; Pêcher and Le Fort, 1986; Hubbard and Harrison, 1989; Coleman, 1996; Hodges et al., 1996; Vannay and Hodges, 1996; Grasemann et al., 1999; Godin et al., 2001; Law et al., 2004). The Tethyan sedimentary sequence structurally overlies the Greater Himalayan sequence, and is defined as an unmetamorphosed to greenschist-facies sedimentary package affected by multiple folding phases with oblique and readily differentiable fabrics and geometries (Colchen et al., 1981;

* Corresponding author. Tel.: +1 613 533 3223; fax: +1 613 533 6592.
E-mail address: godin@geol.queensu.ca (L. Godin).

1367-9120/$ - see front matter © 2005 Elsevier Ltd. All rights reserved.
doi:10.1016/j.jseaes.2005.06.011

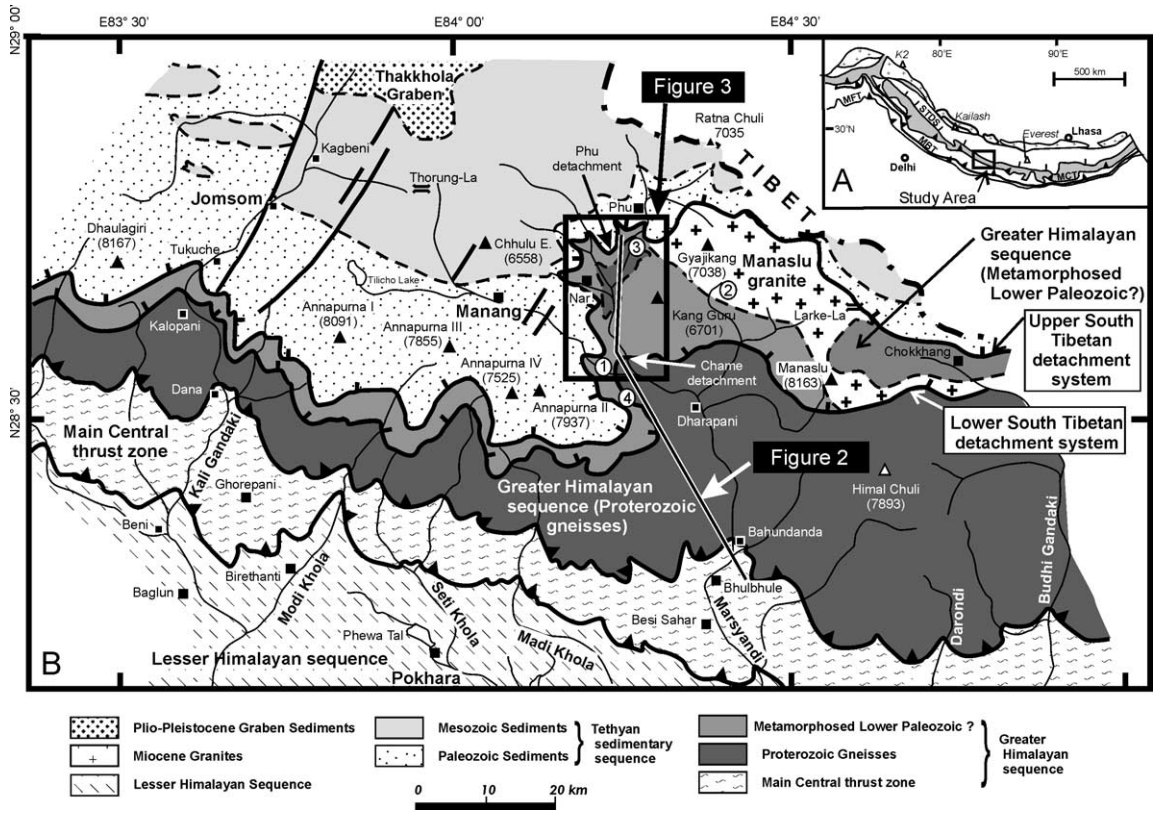

Fig. 1. (A) Study area within the Himalayan orogen. Greater Himalayan sequence in grey and important structures noted are Main Frontal thrust (MFT), Main Boundary thrust (MBT), Main Central thrust (MCT), and South Tibetan detachment system (STDS). (B) Regional geology map modified from Searle and Godin (2003). Sample locations for age constrains: (1) Ar–Ar phlogopite cooling ages (Coleman and Hodges, 1998); (2) U–Th monazite ages from the Manaslu leucogranite (Guillot et al., 1994; Harrison et al., 1999); (3) a U–Pb age of a cross-cutting, yet folded pegmatitic dyke (Godin et al; in press); and (4) a U–Pb age of an undeformed dyke (Coleman, 1998).

Searle et al., 1987; Weismayr and Grasemann, 2002; Godin, 2003). The contact between the metamorphic core and the overlying sedimentary package is the South Tibetan detachment system, a complex transition zone punctuated by north-dipping normal faults (Burg et al., 1984; Burchfiel and Royden, 1985; Burchfiel et al., 1992; Coleman, 1996; Hodges et al., 1996; Searle, 1999).

In the Marsyandi valley of central Nepal (Fig. 1), previous studies of the transition between the Greater Himalayan sequence and Tethyan sedimentary sequence offer contradictory interpretations, from conformable (Fig. 2(A); Bordet et al., 1975; Colchen et al., 1981) to ductile Chame detachment (Fig. 2(B); Coleman, 1996; Coleman and Hodges, 1998). Yet, petrography and thermometry of the same transition zone suggest there is no clear metamorphic discontinuity present (Schneider and Masch, 1993). The Chako dome is located north of the Chame detachment, in the Nar valley. It was originally mapped as a metamorphic culmination protruding through the Tethyan sedimentary sequence (Fig. 2(A); Bordet et al., 1975; Colchen et al., 1986). The geometry and timing of a metamorphic dome in the immediate hanging wall of the detachment fault implies complicated space problems (Godin, 2001). Le Fort et al. (1999) mapped, but did not describe in detail, several normal faults at the top of the metamorphic rocks in the Nar valley (Le Fort and Guillot, 1998). Searle and Godin (2003) recently re-interpreted the rocks above the Chame detachment as Lower Palaeozoic components of the Greater Himalayan sequence, and mapped the brittle Phu detachment, a second major strand of the South Tibetan detachment system 1.5 km structurally above the Chame detachment (Fig. 2(C)). This interpretation positions the Chako dome area within the Greater Himalayan sequence, structurally below the uppermost South Tibetan detachment fault.

The objective of this study is to reconcile these previous interpretations, and to simplify the nomenclature used in central Nepal. This paper details the style of important structural and metamorphic discontinuities, and applies clear lithotectonic definitions to the Greater Himalayan sequence and the Tethyan sedimentary sequence, based on integrated lithological, structural, and metamorphic descriptions. The nature and evolution of the discontinuities are interpreted from detailed mapping, structural analysis, and metamorphic petrology. Our study correlates rock units and re-defines an expanded Greater Himalayan sequence (Fig. 2(D)). A cohesive regional tectonometamorphic model of the transition zone between metamorphic core and overlying sediments reconciles the geometry and timing of the Chako dome and the Chame detachment.

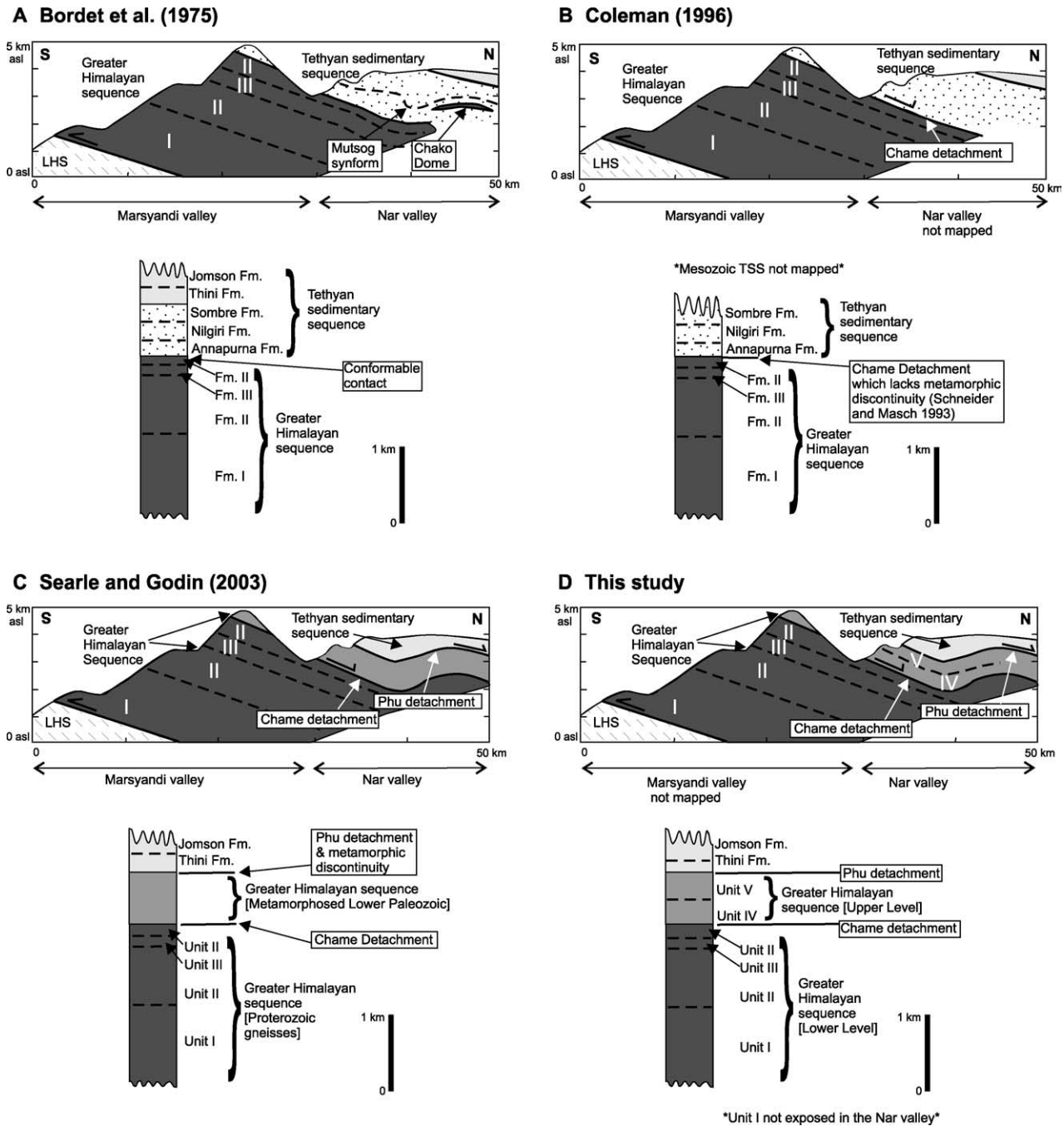

Fig. 2. Simplified cross-sections and structural columns showing interpretations and nomenclature of previous workers and this study. The major tectonostratigraphic units are the Lesser Himalayan sequence (LHS), the Greater Himalayan sequence, and the Tethyan sedimentary sequence. Rock unit symbols follow Fig. 1; important formations within the Tethyan sedimentary sequence are noted in the structural sections. (A) Bordet et al. (1975) interpreted the contact between the Tethyan sedimentary sequence and the Greater Himalayan sequence as conformable. (B) Coleman (1996) interpreted the contact as the Chame detachment, the sole segment of the South Tibetan detachment system although petrography and thermometry suggest the transition zone is not a metamorphic discontinuity (Schneider and Masch, 1993). (C) Searle and Godin (2003) interpreted rocks above the Chame detachment as part of the Greater Himalayan Sequence. (D) This study expands the nomenclature of the Greater Himalayan sequence to include Units IV and V.

2. Geology of the Annapurna region

The Annapurna region is a classic, well-studied transect through the central Himalayan orogen (Bordet et al., 1975; Le Fort, 1975; Colchen et al., 1986; Le Fort et al., 1987; Fuchs et al., 1988; Gradstein et al., 1992; Brown and Nazarchuk, 1993; Garzanti et al., 1994; Coleman, 1996; Hodges et al., 1996; Vannay and Hodges, 1996; Coleman and Hodges, 1998; Garzanti, 1999; Godin et al., 1999a,b, 2001; Le Fort et al., 1999; Godin, 2003; Searle and Godin, 2003). Similar to other Himalayan regions, the Greater Himalayan sequence in the Annapurna region is flanked by two lesser metamorphosed lithotectonic units and bound by north-dipping Cenozoic fault systems (Gansser, 1964; Hodges, 2000; Yin and Harrison,

2000). Our study area is located at the transition between the Greater Himalayan sequence and the structurally overlying Tethyan sedimentary sequence, which is marked by the South Tibetan detachment system. Structurally below our study area, the Main Central thrust carries the Greater Himalayan sequence over the Lesser Himalayan sequence (Le Fort, 1975; Bouchez and Pêcher, 1981; Hubbard, 1996).

2.1. The Greater Himalayan sequence

The Greater Himalayan sequence consists of Proterozoic to Palaeozoic sedimentary and granitic rocks, polydeformed and metamorphosed at amphibolite to granulite facies (Le Fort, 1975; Pêcher, 1989; Burchfiel et al., 1992; Hodges, 2000). In the Annapurna region, the Greater Himalayan sequence has been traditionally divided into three lithologicaly distinct packages: Formation I, Formation II, and Formation III (Fig. 2(A); Colchen et al., 1986). Searle and Godin (2003) used the term 'unit' rather than 'Formation' because these 'Formations' are interlayered, metamorphosed and deformed (Fig. 2(C)). Unit I consists of interlayered kyanite-sillimanite grade pelitic schist, gneiss and migmatite. Unit II is a heterolithic package of calc-silicate gneiss, marble and psammitic schist and gneiss. The dominant and most distinctive lithology of unit II is a calc-silicate gneiss with dark diopside-hornblende-biotite rich layers and light quartz–feldspar–calcite rich layers (Coleman, 1996; Hodges et al., 1996). Unit III is an interlayered biotite schist and Ordovician augen orthogneiss, characterised by 1–4 cm feldspar augens (Bordet et al., 1975; Hodges et al., 1996; Godin et al., 2001). A possible protolith for the meta-sedimentary rocks of the Greater Himalayan sequence is the lower Tethyan sedimentary sequence (Vannay and Grasemann, 2001; Gehrels et al., 2003; Searle and Godin, 2003). Synmetamorphic leucogranites, including the Manaslu leucogranite and various smaller bodies and dykes, intrude the Greater Himalayan sequence (Guillot et al., 1993; 1994; Hodges et al., 1996; Harrison et al., 1999).

The Greater Himalayan sequence is characterised by high-grade metamorphism and south-verging transposition deformation. Above the Main Central thrust, peak metamorphic temperature increases structurally upwards from 550 to 750 °C through an inverted isograd sequence (Vannay and Hodges, 1996). The upper part of the Greater Himalayan sequence exhibits a normal isograd sequence (Le Fort, 1975; Coleman, 1996; Godin et al., 2001). Calcite–dolomite solvus thermometry of the uppermost Greater Himalayan sequence suggests peak metamorphic temperatures of >510 °C (Schneider and Masch, 1993). Peak metamorphic pressures suggest burial greater than ~ 35 km during metamorphism (Vannay and Hodges, 1996). Syn-metamorphic to post-metamorphic deformation within the Greater Himalayan sequence produced pervasive ductile high strain zones, a homoclinal north-dipping transposition foliation, and meso- to microscopic south-verging structures (Pêcher, 1975; Pêcher and Le Fort, 1986; Brunel, 1986; Hodges et al., 1996). Folds at all scales are tight to isoclinal, and are commonly asymmetric with a south vergence (Coleman, 1996; Godin et al., 2001). Microstructural shear-sense indicators suggest general non-coaxial strain and include mantled porphyroblasts, mica fish, C′ planes and S-C fabrics (Bouchez and Pêcher, 1981; Brunel and Kienast, 1986; Nazarchuk, 1993).

2.2. The Tethyan sedimentary sequence

The Tethyan sedimentary sequence consists of Cambro-Ordovician to Tertiary sediments deposited on the northern passive margin of the Indian paleocontinent (Gaetani and Garzanti, 1991; Gradstein et al., 1992; Garzanti, 1999). In the Annapurna region, the lowest exposed Tethyan sedimentary sequence unit is the Sanctuary-Pi Formation, a 500 m thick package of heterogeneous biotite-muscovite schist and metamorphosed sandstone (Colchen et al., 1986; Gradstein et al., 1992; Garzanti, 1999). Overlying the Sanctuary-Pi Formation is the Ordovician carbonate sequence of the Annapurna-Yellow Formation and the Nilgiri Formation (Colchen et al., 1986). The Annapurna-Yellow Formation is a 800 m thick psammite with muscovite and phlogopite defining the foliation, giving the formation its pale yellow patina (Bordet et al., 1975). The Nilgiri Formation is a 1500 m thick, massive, brachiopod-rich, unmetamorphosed limestone (Bordet et al., 1975). The North Face quartzite forms the upper 400 m of the Nilgiri Formation and includes calcareous arkoses and siltstones (Coleman, 1996). Overlying the Ordovician sequence are shales and gritty limestones of the Silurian-Devonian Sombre Formation and black shales and massive limestones of the Permo-Carboniferous Lake Tilicho and Thini Chu Formations (Colchen et al., 1986). The massive Triassic to Jurassic carbonate sequences of the Thini, Jomsom, and Bagung Formations are overlain by the Late Jurassic Lupra Formation shales (Gradstein et al., 1992).

The deformation and metamorphism of the Tethyan sedimentary sequence distinguish it from the Greater Himalayan sequence. The Tethyan sedimentary sequence commonly exhibits multiple folding phases with cross-cutting and readily differentiable fabrics, but lacks high strain zones and transposition foliation (Colchen et al., 1981; Godin, 2003). The lowermost Tethyan sedimentary sequence is metamorphosed to zeolite or lowest greenschist grade with a foliation typically outlined by muscovite. The metamorphic grade decreases upwards to the epizone-anchizone boundary (Garzanti et al., 1994). As a lithotectonic unit, the Tethyan sedimentary sequence *senso stricto* is considered an unmetamorphosed sedimentary package (Gansser, 1964; Hodges, 2000).

2.3. The South Tibetan detachment system

The nature of the contact between the Greater Himalayan sequence and the Tethyan sedimentary sequence in the Annapurna region is complex. Early workers interpreted the contact as conformable because they found similar rock types and metamorphic grades on either side (Bordet et al., 1975; Colchen et al., 1986). However, the contact marks a clear break in structural styles. Detailed mapping reveals families of top-

down-to-the-north high strain zones, called the South Tibetan detachment system, near or at the upper boundary of the Greater Himalayan sequence (Caby et al., 1983; Brown and Nazarchuk, 1993; Hodges et al., 1996; Godin et al., 1999a). In the Marsyandi valley, Coleman (1996) mapped the Chame detachment as a part of the South Tibetan detachment system with an orogen-perpendicular strike (Fig. 1). The Chame detachment juxtaposes unit II of the Greater Himalayan sequence in its footwall against the metamorphosed Nilgiri Formation in its hanging wall (Coleman, 1996; Coleman and Hodges, 1998). The peak metamorphic temperature inferred from prograde assemblages and calcite–dolomite geothermometry are indiscernible across the contact (Schneider and Masch, 1993). Recent work suggests that the South Tibetan detachment system consists of a lower, ductile Chame detachment and an upper, brittle Phu detachment (Searle and Godin, 2003). The ductile segment defines a structural break and is coeval ($\sim$22 Ma) with Neohimalayan metamorphism (Coleman, 1998). The brittle segment is younger ($<$19 Ma) and defines the metamorphic break between the Greater Himalayan sequence and the Tethyan sedimentary sequence.

3. Geology of the Nar valley

The Nar valley was previously interpreted as predominantly Tethyan sedimentary sequence with a small protruding dome of metamorphosed Greater Himalayan sequence (Fig. 2(A); Bordet et al., 1975; Colchen et al., 1986). In this study, the Nar valley is re-interpreted as predominantly Greater Himalayan sequence with an overlying cap of Tethyan sedimentary sequence (Fig. 2(D)). The Greater Himalayan sequence in the Nar valley is divisible into a Lower Level and an Upper Level based on lithology, structures and metamorphic grade (Figs. 3 and 4). Lower Level units correlate with the Greater Himalayan sequence exposed in the Marsyandi valley. The Lower Level is an interlayered package of two rock types: unit II hornblende-biotite schist and unit III, a biotite schist with pods of augen gneiss. Unit I is not exposed in the Nar valley. Lower Level units are intruded by numerous pegmatitic dykes. The Upper Level, originally described as Tethyan sedimentary sequence by Bordet et al. (1975), consists of a micaceous marble (unit IV) and a garnet phyllite-schist (unit V). As such, it is re-interpreted as a previously undescribed part of the Greater Himalayan sequence based on metamorphic constraints, described below. Upper Level rock types cannot be directly correlated with previously described components of the Greater Himalayan sequence in the Annapurna region. Therefore, we suggest expanding the nomenclature of the Greater Himalayan sequence in Central Nepal to include unit IV and unit V of the Upper Level, in accordance with recent interpretations of Searle and Godin (2003).

Map patterns within the Nar valley are controlled by a map-scale antiform-synform pair, and by topography (Fig. 3). The 'bull's eye' map pattern of the Lower Level, previously described as the Chako dome, is controlled by a large west-plunging antiform (Chako antiform) with superimposed north-south drainage (Bordet et al., 1975). The Upper Level outcrops predominantly in the southern portion of the map area, in the core of a west-plunging synform (Mutsog synform). The Manaslu leucogranite outcrops north of the map area. This section describes the lithology, thickness, mineralogy and texture of each unit of the Lower and Upper Levels, as well as the overlying Tethyan sedimentary sequence units exposed in the Nar valley.

3.1. Unit II: Hornblende-biotite schist

Two indistinguishable layers of pistachio to dark green weathering hornblende-biotite schist comprise unit II and are separated by a layer of unit III biotite schist (Fig. 4). Unit II consists of a $\sim$2000 m thick upper layer and a $>$600 m thick lower layer. Well-layered, transposed foliations at lower structural levels grade into massive, mottled schist at higher structural levels. Primary and retrogressed layers are interlayered at millimetre- to centimetre-scale in the well-layered schist. The massive schist is characterized by anastomosing foliations devoid of compositional interlayering. Variations in the mineralogy and texture of unit II are controlled by retrograde replacement and transposition by high strain zones.

3.2. Unit III: Biotite schist and augen gneiss

Unit III is a banded black and white biotite schist containing pods of augen gneiss. Unit III is a $\sim$650 m layer flanked above and below by unit II schist. The mineral assemblage consists of biotite + quartz + titanite $\pm$ hornblende $\pm$ plagioclase with rare chlorite $\pm$ k-feldspar $\pm$ muscovite. The foliation of this mica-rich lithology is outlined by biotite, and locally by proto-gneissic compositional layering. Three pods of coarse grained, white granitic augen gneiss are found within unit III (Fig. 3). The pod above Chako is $\sim$200 m thick and the two pods near Dzonum are 5–10 m thick. The gneiss contains conspicuous 2–5 cm long feldspar porphyroclasts. The biotite schist and augen gneiss consistently outcrop together in the Nar valley and the Marsyandi valley. In a 1–2 m contact above Chako, the augen gneiss progressively becomes finer grained, grading into the biotite schist. Outcrop patterns, grain size and mineralogical similarities suggest that the biotite schist is a high strain equivalent of the augen gneiss. Unit III is interpreted as an Ordovician granite intruding unit II before Himalayan deformation, as documented elsewhere in the Greater Himalayan Sequence (Godin et al., 2001; Gehrels et al., 2003).

3.3. Unit IV: Phlogopite marble

Unit IV is a yellow–grey weathering biotite to phlogopite marble. It is a 500 m thick recrystallised, unfossiliferous marble (Fig. 4). The foliation is outlined by moderately well developed phlogopite and biotite partings with recrystallised intrafolial calcite.

3.4. Unit V: Garnet-biotite phyllite and schist

Unit V consists of silver to black phyllite and schist. It is a 500 m thick unit lying above unit IV. Garnet

porphyroblasts (1–3 mm) differentiate this unit from others. Unit V is interlayered at the decimetre-scale with phyllite and schist layers and locally gneiss layers near Chhacha (Fig. 3). In all cases the foliation is outlined by biotite and muscovite. Poorly preserved fossils within unit V provide broad depositional and age constraints. The phyllite locally contains 2–3 mm pelmatazoan echinoderms, which restrict deposition of unit V to the Phanerozoic, likely a back

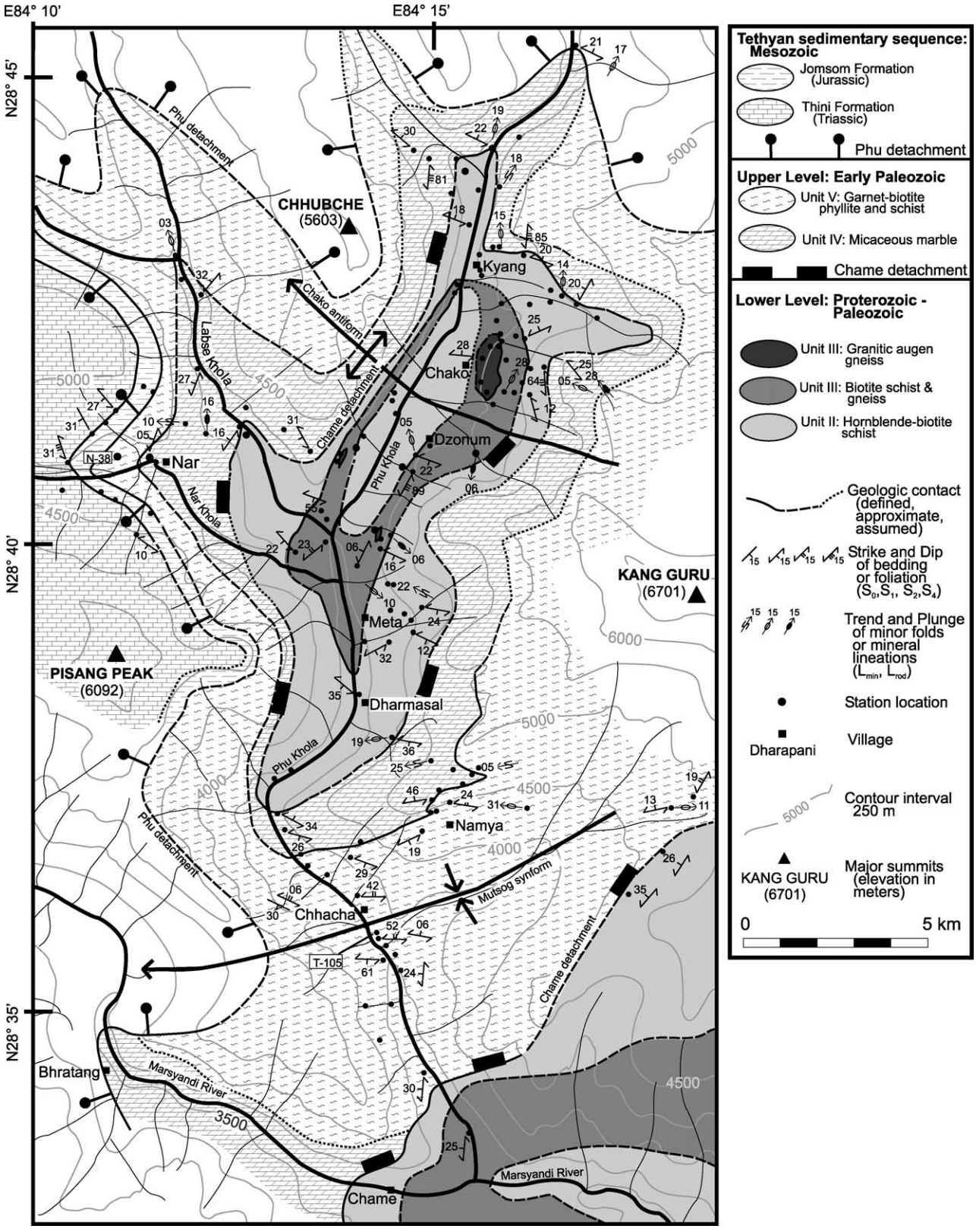

Fig. 3. Geology map of the lower Nar valley. Geology of the Marsyandi valley modified from Coleman (1996).

lagoon to lower slope depositional environment (T. Beatty pers. comm. 2003).

3.5. The Tethyan sedimentary sequence

Above the village of Nar, the Tethyan sedimentary sequence consists of two unmetamorphosed units above the unit V (Fig. 3). The Upper Triassic Thini Formation is a >200 m thick, black to grey shale (Colchen et al., 1986). The Lower Jurassic Jomsom Formation is a ~500 m thick, grey to dun micritic limestone (Colchen et al., 1986). A mountain-scale anticline, visible in the cliffs above Nar village, overturns this stratigraphy (Bordet et al., 1975; Colchen et al., 1986).

4. Structural geology

The Lower and Upper Levels, separated by the Chame detachment, are characterized by different structures, especially D_2 features (Fig. 3). In the Lower Level, D_2 strain is partitioned into distinct, transposed high strain zones with intermediary ductile flow folds. In the Upper Level, D_2 strain is accommodated by chevron to cuspate folds. Structures characterising the two structural levels are described separately for the early deformation (D_1 and D_2). We suggest that the Upper Level was deformed at considerably higher structural levels than the Lower Level and that the early deformation may not be coeval in those two structural levels.

Both the Upper and Lower Levels are characterised by an early, foliation-producing event (D_1); a folding and locally foliation-producing event (D_2); crustal-scale large amplitude folding (D_3); and a late, brittle faulting and fracturing event (D_4). D_1 and D_2 features in the Lower Level are differentiated using the subscript 'L' for lower (i.e. D_{1L}). D_1 and D_2 features in the Upper Level are then described and differentiated using the subscript 'U' for upper (i.e. D_{1U}). D_3 and D_4 deformation phases are not assigned to a specific level because they affect both Lower and Upper Levels.

4.1. Lower level early structures

In the Lower Level, the first two generations of structures are D_{1L} foliations, and D_{2L} folds with associated transposition and strain localisation fabrics. S_{1L} is the main planar fabric and a product of D_{1L} deformation (Fig. 5). S_{1L} is a penetrative foliation defined by aligned cleavage domain minerals (biotite ± hornblende ± muscovite; Fig. 5), compositional layering within unit II hornblende-biotite schist, and a weak quartz grain shape foliation and quartz ribbons within unit III augen gneiss (Fig. 6(A)).

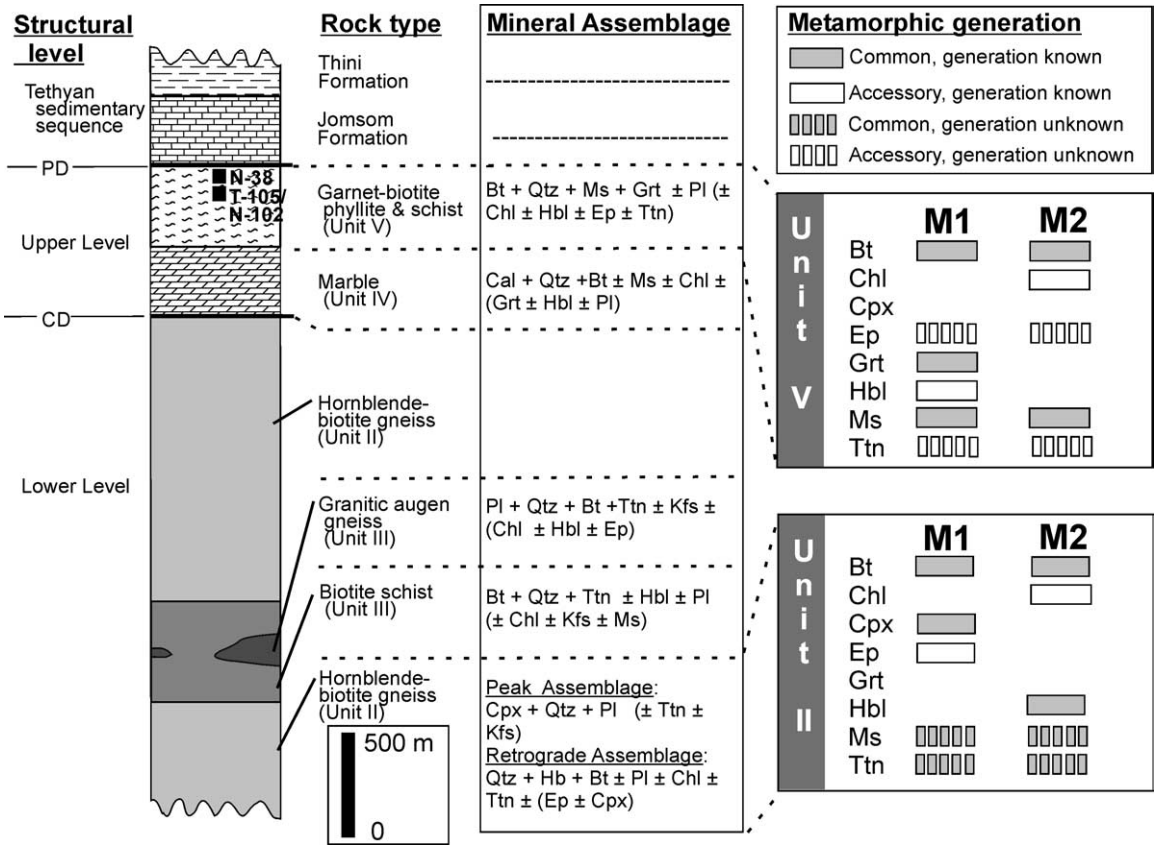

Fig. 4. Mineral assemblages from the different structural levels with accessory minerals in brackets. Metamorphic generations for each level based on textural relations and evidence for metamorphic reactions. Structural levels are separated by the Chame detachment (CD) and the Phu detachment (PD). Mineral abbreviations after Kretz (1983): Bt, biotite; Chl, chlorite; Cpx, clinopyroxene; Ep, epitode; Grt, garnet; Hbl, hornblende; Kfs, k-feldspar; Ms, muscovite; Pl, plagioclase; Qtz, quartz; and Ttn, titanite.

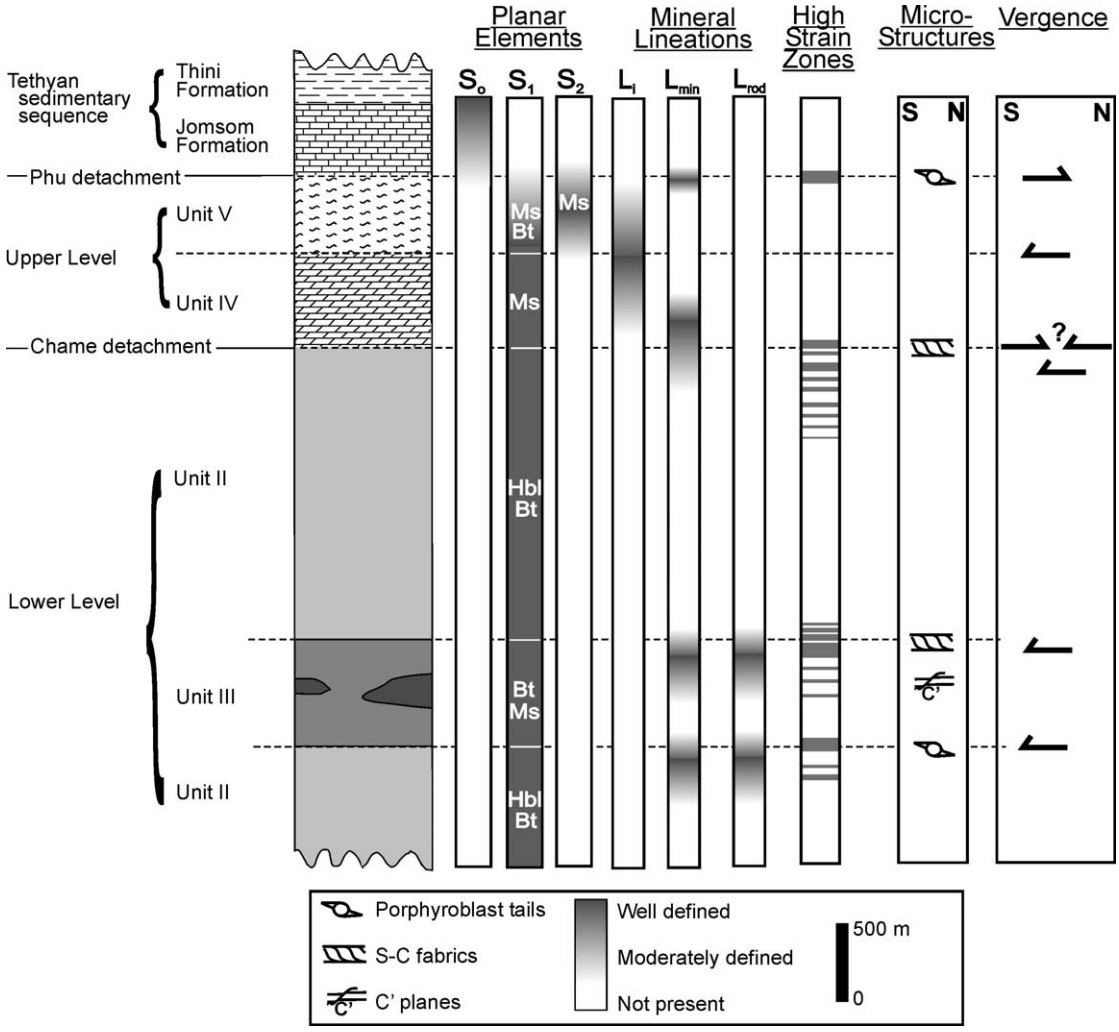

Fig. 5. Summary of the microstructures, planar and linear features at different structural levels. High strain zones contain a well developed planar fabric and a weak to moderate lineation. Mesostructures and microstructures (located within high strain zones) together give sense of vergence. Dominant phase of fabric definition at different structural levels are noted with mineral abbreviations after Fig. 4. L_i, intersection lineation of S_1 and S_2; L_{min}, mineral aggregate lineation; L_{rod}, mineral rod lineation.

D_{2L} is partitioned into 1–100 m thick high strains zones with intermediary lower strain zones (Fig. 5). High strain zones are characterised by an intense transposition foliation (S_{2L}) affecting S_{1L}, development of mineral lineation (L_{rod} and L_{min}), and a higher concentration of shear sense indicators. High strain zones are concentrated at contacts, suggesting that rheological contrasts control their localisation (Fig. 5). Between high strain zones, the rocks exhibit anastomosing fabrics, and lack mineral lineations and shear sense indicators. Macroscopic folds, which are common between high strain zones, have not been observed within the high strain zones.

Mineral lineations on S_{2L} surfaces commonly develop within high strain zones. Quartz mineral rods are rare mineral elongation lineations (L_{rod} on Figs. 5 and 7). Mineral aggregate lineations of biotite and hornblende are more common (L_{min} on Figs. 5 and 7). Both types of lineation show a large dispersal of trends with a mean orientation plunging 14° towards N333° (Fig. 7(G)). However, the limited data set precludes statistical interpretation. No lineation cross-cutting relationships were observed, suggesting all the lineations are part of the same generation. Lineations are interpreted as coeval to D_{2L} because they are only developed in D_{2L} high strain zones. Lineations may have been dispersed due to variable rotation during transposition, or to a pure shear component, as described below.

A high concentration of asymmetric and symmetric D_{2L} structures characterises the high strain zones. The presence of both asymmetric and symmetric shear sense indicators visible on surfaces parallel to observed lineations and perpendicular to the foliation suggest general non-coaxial flow. Asymmetric features that verge south include well developed sigma porphyroblasts (Fig. 8(A)) and poorly developed C-S fabrics and C′ shear bands. Pervasive folds are open to closed, centimetre-scale to metre-scale and overturned to the south with fold hinge lines plunging 08° towards N300° (Fig. 7(F)). The folds are elliptical to teardrop shaped, suggesting ductile flow during folding. Common symmetric structures are symmetric strain shadows and alpha tails on diopside porphyroblast and feldspar porphyroclasts.

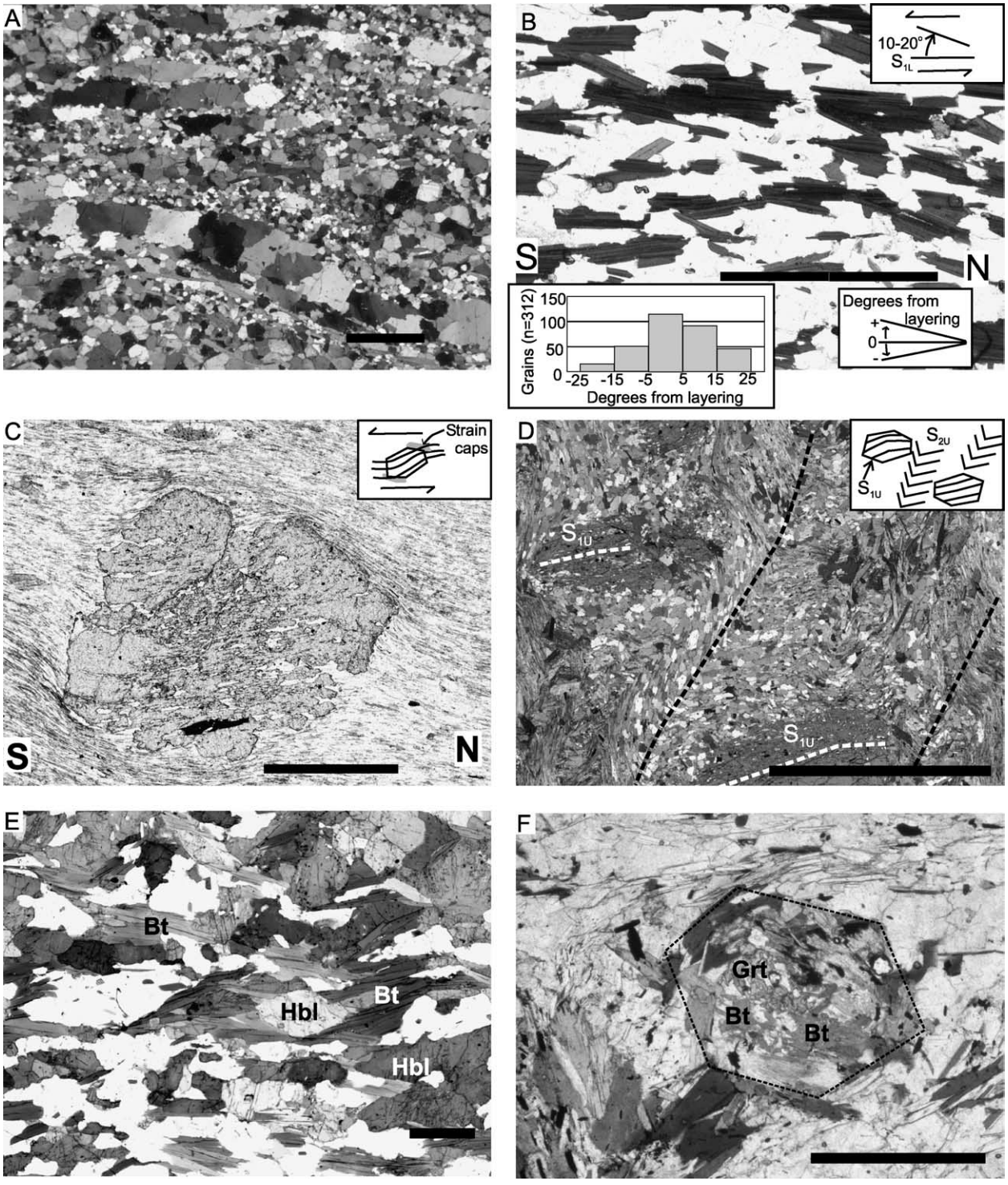

Fig. 6. Thin section microstructures with geometric and kinematic interpretations. (A) quartz ribbons in Unit III; (B) biotite composite fabric in Unit II; note histogram of biotite long axes orientation relative to compositional layering possibly indicative of strain insensitive fabric consistent with south-verging ductile flow; (C) rotated garnet porphyroblast in Unit V schist; (D) S_1 and S_2 fabrics developed in Unit V; (E) biotite enclosing hornblende in Unit II; and (F) biotite pseudomorph of garnet in Unit V. All scales are 2 mm. All sections are cut parallel to the lineation, and perpendicular to the dominant foliation except thin sections (A) and (D) are not oriented.

Between high strain zones, asymmetric folds and composite fabrics are developed. The asymmetric folds between high strain zones have a similar style and orientation to the asymmetric folds within high strain zones, however, they have an amplitude up to 20 m (Fig. 8(B)). Unit III biotite schist shows a composite fabric defined by biotite grains (Fig. 6(B)). The orientation of the biotite long axis relative to the compositional layering indicates a degree of asymmetry with grains preferentially oriented top-down-to-the-northwest (Fig. 6(B)). The composite biotite fabric cannot be linked

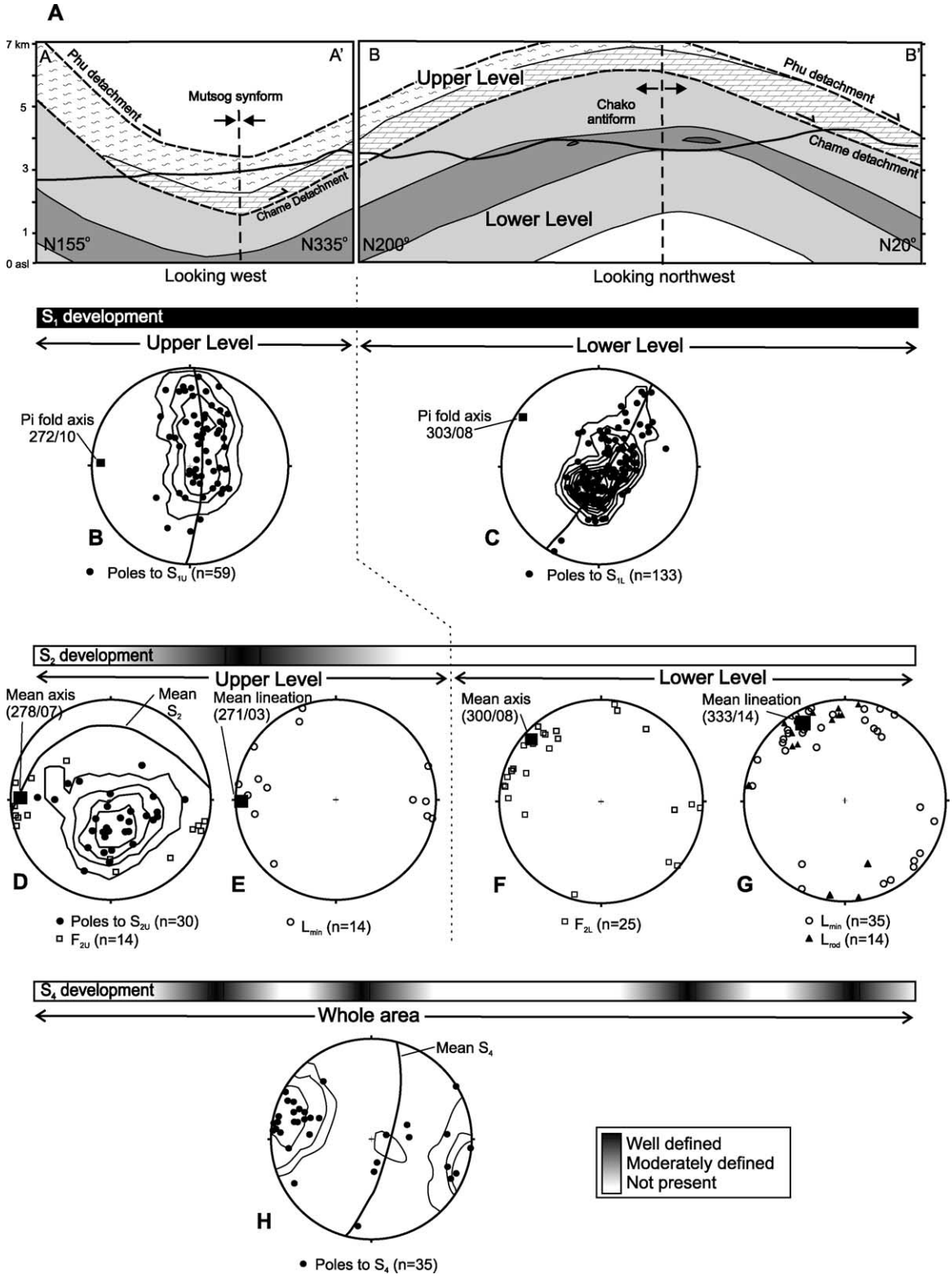

Fig. 7. (A) Composite cross-section along the section line shown on Fig. 3; structural interpretation above 5 km above sea level based on down-plunge projection of geology to northwest. Lithology symbols after Fig. 3. The location and intensity of fabric development for each deformation phase are shown by the shading on section-parallel bars. For the Lower Level, S_{1L} and S_{2L} are parallel and undifferentiated. For the Upper Level, S_{1U} and S_{2U} are oblique and differentiated. Fold axis calculated as mean eigenvectors of F_{2L} and F_{2U} axes or π poles of S_1 fabrics. Equal area stereonets with planar features plotted with two sigma uncertainty.

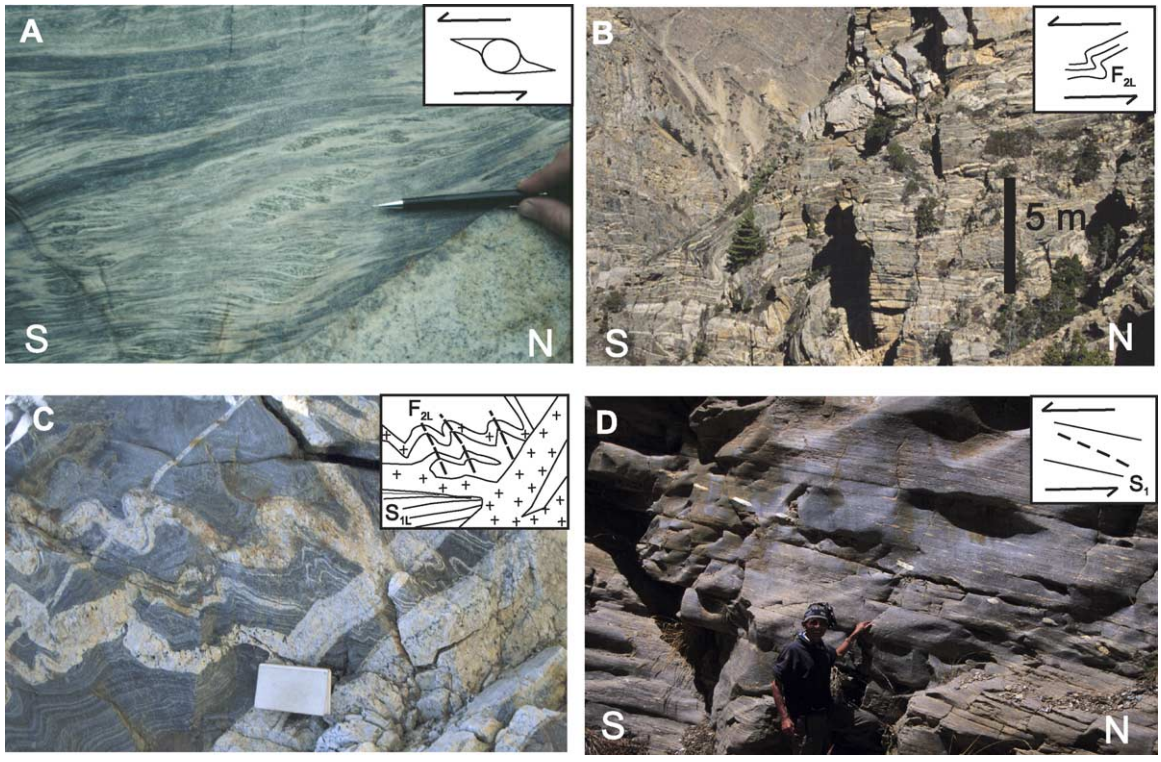

Fig. 8. Outcrop appearance of mesostructures; all views looking west except (C) which is not oriented. (A) σ porhyroblasts in Unit II horneblende-biotite schist; (B) asymmetric folds in Unit III biotite schist; (C) synkinematic dyke relationships in Unit III near Meta; and (D) rotated boudin trail at Lower–Upper Level contact north of Kyang village. Pencil and notebook are both approximately 15 cm in length.

with observable C-S fabrics. We interpret these as representing a composite strain-insensitive fabric (Hanmer, 1984), or a poorly developed S_{2L} axial planar cleavage (Davis and Reynolds, 1996), both indicating south vergence.

Two generations of pegmatitic dykes intrude the Lower Level: a layer-parallel generation, and a cross-cutting, south-dipping generation. The dykes provide age constraints and are most common in the unit III biotite schist, locally comprising up to 40% of unit III volumetrically. The mineral assemblage of the pegmatitic dykes consists of quartz + plagioclase + hornblende ± k-feldspar ± tourmaline ± muscovite. The first generation is boudinaged parallel to S_{1L} fabrics. The second generation cuts across S_{1L} fabrics at high angles and consistently dips to the south. The consistent dip of the cross-cutting dykes is interpreted to reflect the extensional field of the regional strain ellipse at the time of emplacement, suggesting south-directed deformation. At an outcrop-scale, complex intrusive relationships suggest the second generation is synkinematic to D_{2L} deformation (Fig. 8(C)). The age of the second generation of dykes (U–Pb concordant zircon at 19.9 ± 0.1 Ma; Godin et al. in press) is thus interpreted as the minimum age of D_{1L} deformation and the maximum age of D_{2L} deformation (Godin, 2001).

4.2. Upper level early structures

In the Upper Level, the first two structural generations are a D_{1U} foliation-producing event and a D_{2U} folding event. S_{1U} is the main planar fabric defined in units IV and V of the Upper Level (Fig. 5). Within the unit IV micaceous marble, S_{1U} is defined by aligned muscovite ± biotite grains (Fig. 5) and a weak calcite grain shape foliation. Unit V is texturally variable from phyllite to schist to, locally, gneiss. The continuous to spaced S_{1U} foliation of unit V is defined by muscovite ± biotite.

In unit V, sub-euhedral to euhedral, 1–3 mm garnets contain an internal foliation outlined by inclusion trails, which are continuous with S_{1U} cleavage outside the porphyroblast (Fig. 6(C)). Based on this continuity and the curvature of inclusion trails, both of which are evidence for porphyroblast modification during growth, the garnet growth is interpreted as coeval with the development of the S_{1U} phyllitic cleavage. The curved inclusion trail and cleavage outside the porphyroblasts suggest syntectonic growth during southward rotation relative to the cleavage. A southward-verging kinematic interpretation is further supported by common strain caps (Passchier and Trouw, 1998) in the upper-north and lower-south corners of the garnets (Fig. 6(C)).

In the Upper Level, D_{2U} deformation is characterised by asymmetric folds, and the development of S_{2U} axial planar cleavage and hinge-parallel mineral lineations, which affect the S_{1U} foliation. The folds are open to closed, centimetre- to metre-scale and overturned to the south with a mean fold hinge plunging 07° towards N278° (Fig. 7(D)). Upper Level folds exhibit angular hinge zones and chevron fold shapes, especially in unit V, suggesting that they formed at higher structural levels than Lower Level folds of the same generation. The S_{2U} foliation is a crenulation cleavage developed axial planar to F_{2U} folds, dipping north and defined by aligned biotite

and muscovite (Figs. 5 and 7(D)). Biotite and muscovite mineral aggregates define a mineral lineation with a mean orientation plunging 03° towards N271° (L_{min} on Figs. 5 and 7). The mineral lineations are quite dispersed. However, Upper Level mineral lineations are considered coeval to D_{2U} deformation because their orientations are similar to F_{2U} fold axis (Fig. 7(D)) and to rare S_{1U}–S_{2U} intersection lineations.

4.3. Northern extent of the Chame detachment

Structural, metamorphic, and age constraints indicate that the contact between the Lower and Upper Levels in the lower Nar valley is the northern extension of the Chame detachment. Composite cross-sections illustrate that the contact between the Lower and Upper Levels is at the same structural position as the Chame detachment, with similar hanging wall and footwall rock types (Fig. 7(A)). Metamorphic constraints, discussed below, indicate that the contact between the Lower and Upper Levels is not an obvious metamorphic discontinuity, similar to the Chame detachment. Furthermore, structural similarities to the Lower Level, described below, suggest that the contact between the Lower and Upper Levels was active after 20 Ma (Godin et al. in press), contemporaneous to ductile motion along the Chame detachment (24–18 Ma; Coleman, 1998).

The northern extension of the Chame detachment is a high strain zone exposed at three localities in the Nar valley. At each locality, the zone is characterised by a moderately developed transposition foliation with a mineral aggregate lineation. In the south, near Dharmasal, the high strain zone displays decimetre-scale to outcrop-scale, north-verging F_2 asymmetric folds. In the west, below Nar, it exhibits complex microstructures with multiple inclusion tails. In the north, near Kyang, the contact displays a variety of south-verging D_2 shear-sense indicators, including asymmetric folds, C-S fabrics and boudinaged cross-cutting dykes in which the boudin train progressively rotates south towards the flow plane (Fig. 8(D)). The south-verging structures at the northern contact in Kyang may be explained by overprinting of a late, south-verging out-of-sequence thrust, similar to thrust faults documented nearby in the village of Phu (Schill et al., 2003; Searle and Godin, 2003).

D_2 deformation within the Chame detachment have the same characteristics (transposition, mineral lineation and shear sense indicators) as the D_{2L} high strain zones within the Lower Level. Additionally, pegmatite dykes within the contact zone cross-cut S_1 fabrics and are deformed by D_2 structures, similar to the second generation of dykes and D_{2L} structures. The same dykes are absent in the Upper Level. Therefore D_2 deformation within the Chame detachment is considered contemporaneous to D_{2L} deformation within the Lower Level, which is constrained to <20 Ma (Godin et al. in press).

4.4. Late structures affecting lower and upper levels

The Lower and Upper Levels are equally deformed by a pair of megascopic folds (D_3), and by late spaced cleavages (D_4). The megascopic antiform-synform pair controls the outcrop pattern (Fig. 3) and the map-scale S_1 orientations (Fig. 7(B) and (C)). This pair of folds was previously described as the Mutsog synform in the south and as the Chako dome in the north (Bordet et al., 1975; Coleman, 1996). The term Chako antiform is preferred over the Chako dome because there are no east-dipping foliations to suggest the northern structure is a dome. The orientations of fold axes are well constrained with the π fold axis of S_{1L} and S_{1U} foliations. The hinge of the Mutsog synform plunges 10° towards N272° (Fig. 7(B)). The Chako antiform is oblique to the Mutsog synform with a hinge plunging 08° towards N303° (Fig. 7(C)). Cross-section and map constraints suggest both folds are upright, open folds. The amplitude ($\sim$4 km) and wavelength ($\sim$25 km) of the Mutsog synform-Chako antiform implies crustal scale folding. Crustal-scale folding is considered to represent D_3 deformation, since it folds D_2 structures (i.e. the contact between levels) and locally rotates S_{2U} fabrics in the core of the Mutsog synform (Schill et al., 2003).

D_{2L} and D_{2U} features are deformed by a locally developed brittle spaced S_4 cleavage. This cleavage is spaced on millimetre- to centimetre-scale and has minor (<1 cm) offset. The cleavage is oriented north–south with a steep dip. Near Dharmasal, F_{2L} folds are cross cut by a localised southwest-dipping, brittle fault with minor (<1 m) offset.

5. Metamorphic constraints

Metamorphic constraints from the Lower and Upper Levels are described separately since structural features suggest they may have been deformed at different structural levels and/or different times. The metamorphic evolution of both levels is divisible into a peak metamorphic event (M_1) and a retrograde event (M_2). Petrographic constraints on Lower Level metamorphism (M_{1L} and M_{2L}) are presented followed by constraints on Upper Level metamorphism (M_{1U} and M_{2U}). Thermal constraints derived from garnet-biotite thermometry are used to constrain peak metamorphic temperatures.

5.1. Lower level metamorphism

Metamorphic observations for the Lower Level are based primarily on unit II (Fig. 4). The M_{1L} peak metamorphic assemblage consists of clinopyroxene + quartz + plagioclase ± titanite ± k-feldspar. Clinopyroxene, described in the field as diopside, is subprismatic to prismatic. The presence of clinopyroxene may indicate high-grade metamorphism, but the incomplete mineral assemblage precludes thermobarometric studies. Unit II samples exhibit <5 to 100% replacement of clinopyroxene by retrograde metamorphic minerals (M_{2L}). Incipient replacement of clinopyroxene by hornblende and biotite occurs along fractures. In moderately replaced samples, hornblende and/or biotite enclose the remnant clinopyroxene grains. In completely replaced samples, biotite surrounds hornblende, suggesting that biotite is the final retrograde phase. The M_{2L} assemblage of hornblende

and biotite is thus interpreted to have resulted from retrograde metamorphism (Fig. 6(E)).

5.2. Upper level metamorphism

Upper Level petrographic constraints are based on unit V garnet-biotite phyllite and schist. The M_{1U} metamorphic assemblage of unit V consists of biotite + quartz + muscovite + garnet ± plagioclase ± chlorite. The M_{1U} assemblage of garnet, biotite and muscovite suggests upper greenschist or lower amphibolite facies (Yardley, 1991). Unit V phyllite and schist are characterised by 1–4 mm garnet porphyroblasts. The garnets from the unit V phyllite contain bent inclusion trails but do not display growth zones (Fig. 6(C)). However, the garnets from the unit V schist display two distinct growth zones: an inclusion-poor core and an inclusion-rich rim. Within the schist, garnets locally contain bent inclusion trails continuous with S_{1U} outside the garnet. S_{2U} crenulation cleavage folds S_{1U} outside the garnet (Fig. 6(D)). The garnets from the schist are considered coeval with the garnets in the phyllite because they display similar curved inclusion trails and they overgrow the same fabric (both late S_{1U}) within the same unit. Therefore, the garnets from unit V phyllite and schist are interpreted to be syntectonic to D_{1U}.

Biotite pseudomorphing garnet grains are interpreted as part of the M_{2U} retrograde metamorphic event (Fig. 6(F)). Within the same sample, prismatic, unbent, non-undulose biotite and muscovite outlines the S_{2U} crenulation cleavage (Fig. 6(D)). Garnet retrogression is thus interpreted as synchronous to the development of the S_{2U} crenulation cleavage.

5.3. Thermal constraints

Thermometry of garnets paired with biotites from three unit V samples provide peak M_{1U} metamorphic temperature constraints for the Upper Level (methodology in Appendix). Lower Level metamorphic temperatures are unconstrained due to the absence of garnets, most probably due to the bulk composition of the protolith. The garnets from the unit V schist (T-105 & N-102) exhibit two garnet growth zones of inclusion-poor cores surrounded by inclusion-rich rims. Temperatures derived from the cores of garnet paired with biotite inclusions suggest core temperatures of 540–550 ± 50 °C for sample T-105 (Fig. 9(A)). Rim temperatures derived from pairs with adjacent biotite suggest equilibrium at 620–650 ± 50 °C. Temperatures derived from pairs within samples and from T-105 & N-102 are consistent. The garnet from the unit V phyllite (N-38) lacks both garnet growth zones and biotite inclusions. Adjacent biotites were paired with garnet rim values to obtain rim temperatures of 500–530 ± 50 °C (Fig. 9(B)).

Temperatures obtained from the samples mentioned above indicate that Unit V equilibrated at conditions consistent with amphibolite facies, and that the garnets in the schist samples grew during prograde metamorphism. Biotite retrogression can lead to prograde growth patterns, but this seems unlikely since other prograde garnets are documented from the Annapurna region (Arita, 1983; Hodges et al., 1988; Vannay and Hodges, 1996).

6. Discussion

6.1. Unit correlation

We propose a series of correlations linking the metamorphic rocks of the Chako area with those found within the Greater Himalayan sequence, based on mineralogy, texture, and outcrop appearance. As such, the Lower Level units directly correlate with the Greater Himalayan sequence units exposed in the Marsyandi valley. The Chako unit II correlates with

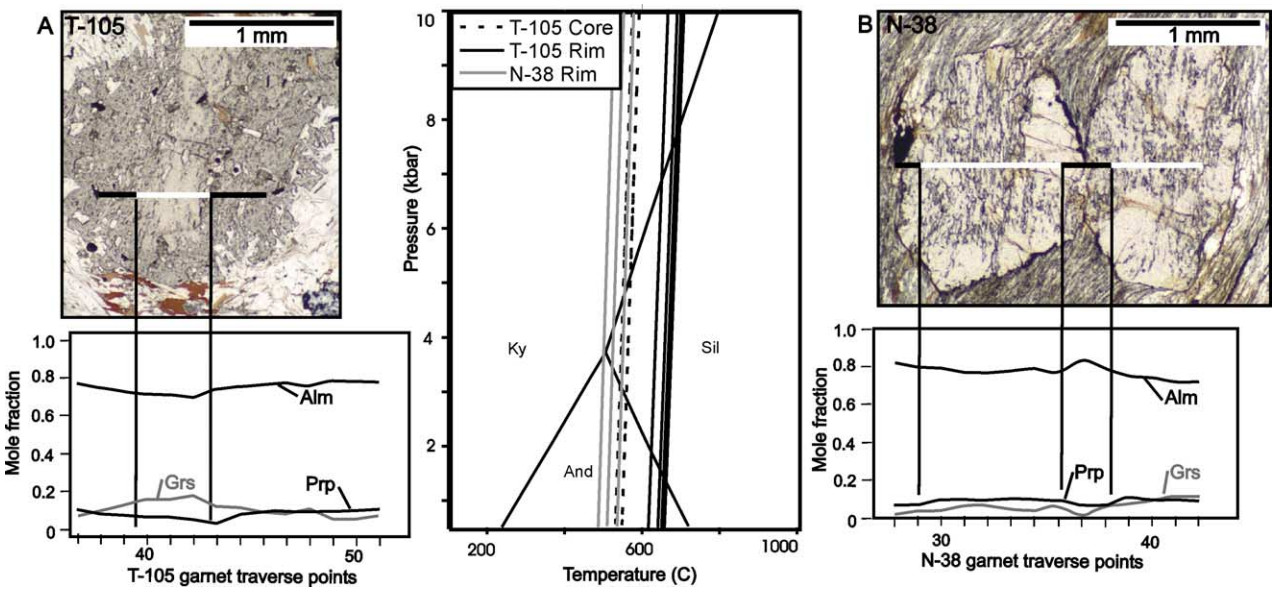

Fig. 9. Garnet traverses with associated zoning profile. Temperatures calculated using TWEEQU (Berman, 1991) for (A) garnet-biotite schist (T-105) and (B) garnet-biotite phyllite (N-38).

unit II calc-silicate schist of the Marsyandi valley (Bordet et al., 1975). Unit II was previously considered a calc-silicate schist because of the presence of calcium minerals, such as diopside (Bordet et al., 1975; Colchen et al., 1986; Godin, 2001). However, the term hornblende-biotite schist is preferred for unit II because of the paucity of carbonate minerals. Unit III biotite schist correlates with the biotite-rich 'gneiss à plaquettes' described by Bordet et al. (1975) based on mineralogy and texture. Colchen et al. (1986) incorporated the biotite schist with a distinct augen gneiss as part of unit III. Therefore, unit III of the Nar valley correlates directly with the unit III granitic augen gneiss found in the Marsyandi valley near Chame (Colchen et al., 1986; Godin, 2001). Similar to the Greater Himalayan sequence elsewhere in the Himalaya, the Lower Level exhibits an early foliation overprinted by south-directed, general non-coaxial high strain zones (Grujic et al., 1996; Grasemann et al., 1999; Law et al., 2004). The predominance of clinopyroxene in peak M_{1L} assemblages suggests high metamorphic grade. Lower Level rock types, structures, and metamorphism, therefore, all suggest they are part of the Greater Himalayan sequence.

We interpret the Upper Level, originally described as Tethyan sedimentary sequence by Bordet et al. (1975), as part of the Greater Himalayan sequence, in agreement with Searle and Godin (2003). Peak metamorphic assemblages and garnet-biotite thermometry suggesting peak metamorphism at upper greenschist to amphibolite facies (500–650 °C) indicate the Upper Level is part of the Greater Himalayan sequence (Hodges et al., 1988; Hubbard and Harrison, 1989; Vannay and Hodges, 1996). However, the Upper Level does not exhibit ductile high strain zones, characteristic of the Greater Himalayan sequence, suggesting its tectonometamorphic provenance may be different from the Lower Level. The nomenclature of the Greater Himalayan sequence in the Annapurna region is expanded to include unit IV and V, because these units cannot be directly correlated with previous unit descriptions.

The Upper Level may have along-strike equivalents in Nepal. In the Everest area, 300 km east of the Marsyandi valley, the Greater Himalayan sequence consists of two structural levels with differing metamorphic grades: structurally lower sillimanite-grade gneisses and sheeted intrusives, and structurally higher Everest Series greenschist rocks with lower intrusive rock content (Searle et al., 2003). In the Kali Gandaki valley, 50 km west of the Marsyandi valley, the Annapurna detachment is a 1.5 km-thick high-strain zone of psammitic composition, which has strong resemblance to the Everest series (Brown and Nazarchuk, 1993; Godin et al., 1999a; Searle and Godin, 2003). The metamorphic grade, rock type, and structural position suggest the Upper Level rock types (unit IV and V) may be equivalent to the Everest Series greenschists and the psammites of the Kali Gandaki valley (Searle et al., 2003; Searle and Godin, 2003). However, detailed mapping indicates that similar units do not outcrop in the Langtang region, intermediary between Everest and Annapurna, or in the Shisha Pangma area, west of the Everest region (Inger and Harris, 1992; Reddy et al., 1993; Searle et al., 1997). If the Upper Level is equivalent to the Everest Series greenschists and the psammites of the Kali Gandaki valley, the lack of equivalent units in the Langtang and Shisha Pangma regions suggests major components of the Greater Himalayan sequence are either discontinuous along strike, or have been cut out by faulting along the upper brittle strand of the South Tibetan detachment system.

6.2. Regional tectonometamorphic model

Fig. 10 presents our suggested field-based tectonometamorphic model based on integrated lithological, structural, metamorphic data and age constraints from previous workers, which reconciles the geometry and timing of the synmetamorphic Chame detachment with the previously interpreted metamorphic dome protruding through unmetamorphosed sediments in its hanging wall (Bordet et al., 1975; Colchen et al., 1986; Schneider and Masch, 1993; Guillot et al., 1994; Coleman, 1996; 1998; Coleman and Hodges, 1998; Harrison et al., 1999; Godin, 2001). We suggest that the Lower and Upper levels experienced early deformation at different structural levels, and were subsequently coupled by the Chame detachment. The Phu detachment subsequently placed the Tethyan sedimentary sequence in contact above the Upper Level, and crustal-scale folds then warped the entire package.

6.3. Pre-20 Ma history

Before 20 Ma, both Upper and Lower levels experienced peak metamorphism and a first phase of deformation, but at markedly different structural levels (Fig. 10(A)). The minimum age of D_{1L}/M_{1L} in the Lower Level is ~20 Ma based on a post-D_{1L} cross-cutting dyke (Godin et al. in press). The timing of D_{1L}/M_{1L} is likely coeval with peak metamorphism of ~22 Ma sillimanite grade gneisses in the Marsyandi valley but could be as old as Oligocene, as described elsewhere in central Nepal (Vannay and Hodges, 1996; Coleman, 1998; Coleman and Hodges, 1998; Godin et al., 2001). The ~20 Ma cross-cutting dyke is also interpreted as a maximum age for Lower Level D_{2L} and movement of the Chame detachment (Godin, 2001). The timing of Upper Level D_{1U}/M_{1U} event is unconstrained because the Upper Level is devoid of leucogranitic dykes, rendering conventional U–Pb geochronology difficult.

The early metamorphism and structures of the Upper Level are better constrained than the Lower Level. In the Upper Level, synkinematic garnet textures reveal that prograde and peak metamorphism (M_{1U}) is coeval with D_{1U} foliation-producing, south-verging deformation (Fig. 10(A)). Metamorphic assemblages and garnet-biotite thermometry suggest M_{1U} reached amphibolite facies (500–650 °C). In the Lower Level, the clinopyroxene-bearing M_{1L} assemblages outline S_{1L} and are coeval with D_{1L} (Fig. 10(A)). However, without thermal constraints for the Lower Level or isograds cross-cutting the two levels, metamorphic data from the two levels are not easily compared.

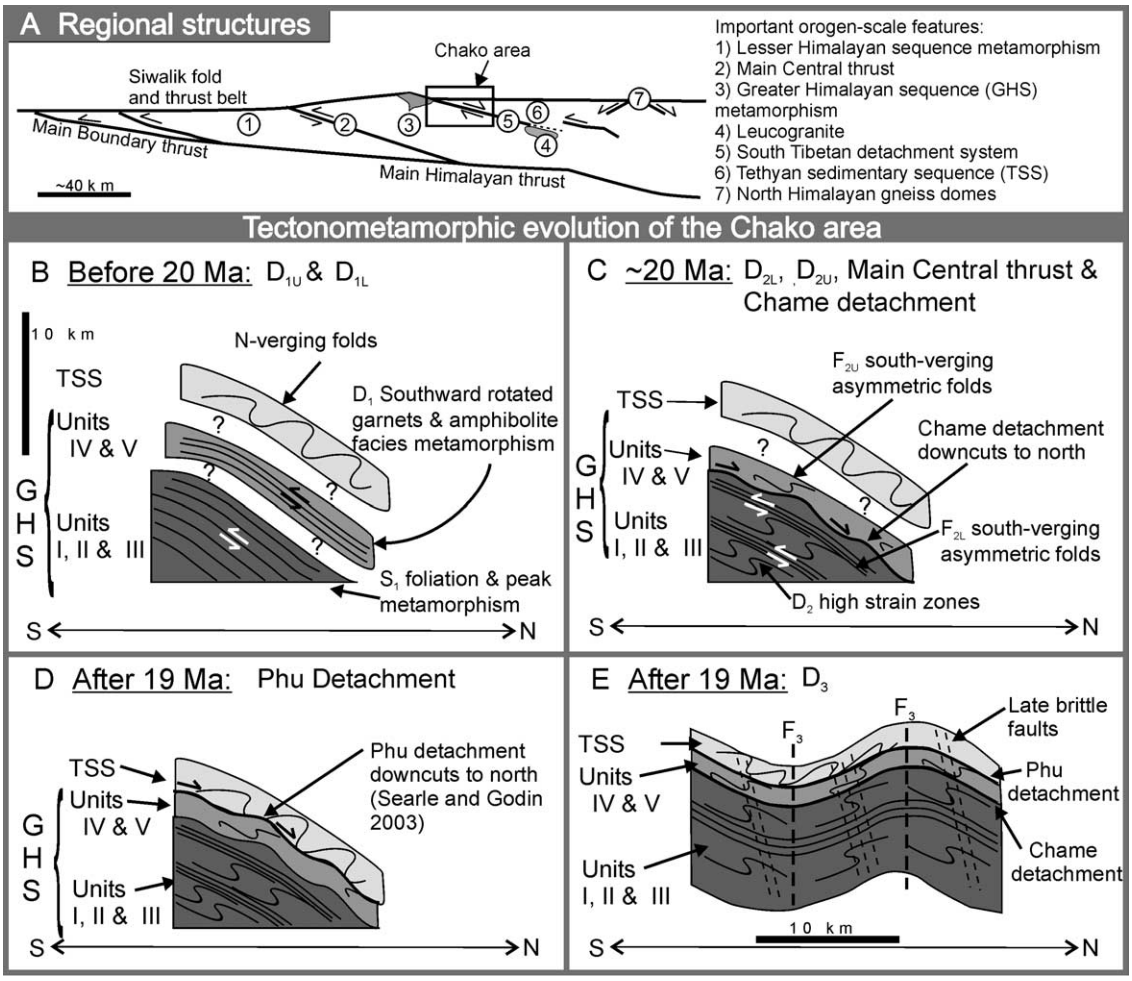

Fig. 10. Simplified cross-sections of regional-scale tectonometamorphic model for central Nepal, placed within framework of regional structures (A). All views look west and the scale is found in (A). Time constraints discussed in text. (B) Early metamorphism and deformation in the Lower and Upper Levels; (C) deformation in the Lower Level, and possibly the Upper Levels, coeval to the Chame detachment, which emplaces the Upper Level on the Lower Level and downcuts to the north; (D) Phu detachment emplaces the Tethyan sedimentary sequence on the Upper Level and also downcuts to the north (i.e. Searle and Godin, 2003); and (E) late crustal-scale folding and subsequent brittle faulting.

6.4. Post-20 Ma history

After 20 Ma, the Chame detachment is interpreted to have emplaced the Upper Level on the Lower Level, possibly during biotite retrograde metamorphism (Fig. 10(B)). The timing of the Chame detachment in the Nar valley is <20 Ma because structural overprinting relationships, fabric transposition and ductile structures suggest the Chame detachment may be correlative to D_{2L} deformation. In the Marsyandi valley, the Chame detachment is a ductile, top-to-the-north shear zone that is syn-metamorphic to peak sillimanite-grade through retrograde greenschist facies metamorphism and active between 22–18 Ma (Coleman, 1998). Cross-section and map constraints suggest that the Chame detachment cuts down to the north through unit V, between Chame and Chhacha (Fig. 7(A); Gleeson, 2003).

In the Upper Level, biotite-muscovite retrograde metamorphism (M_{2U}) is coeval to the development of the shallow north-dipping S_{2U} crenulation cleavage (Fig. 10(B)). The crenulation cleavage is axial planar to south-verging F_{2U} kinks and outcrop-scale folds. The S_{2U} crenulation cleavage is only developed in the Upper Level and is kinematically compatible with formation in the compressional field of the strain ellipse in the hanging wall of a normal fault. The S_{2U} crenulation cleavage may have formed during emplacement of the Upper Level on the Lower Level during biotite-grade retrograde metamorphism in both levels. Alternatively, the S_{2U} crenulation cleavage may have formed during later, renewed south verging deformation (Schill et al., 2003; Searle and Godin, 2003).

In the Lower Level, ductile general shear with a south-directed simple shear component characterises D_{2L} deformation. The relationship between D_{2L} and biotite retrograde metamorphism is unconstrained. D_{2L} is (wholly or partially) younger than $\sim$20 Ma because D_{2L} boundinages and folds leucogranitic dykes dated at ca. 20 Ma. The timing, south-verging asymmetry and transpositional nature of D_{2L} suggest that it may be part of the Miocene Neohimalayan ductile extrusion of the Greater Himalayan sequence.

6.5. Post-19 Ma history

The Phu detachment (Fig. 10(C)) is a recently recognised ductile-brittle normal fault juxtaposing garnet-grade phyllite in its footwall against unmetamorphosed Tethyan sedimentary sequence in its hanging wall (Searle and Godin, 2003). The Phu detachment is interpreted as the upper, brittle strand of the South Tibetan detachment system, which down cuts through previously folded strata. Since the Phu detachment cuts out the northwest part of the Manaslu leucogranite (Searle and Godin, 2003), it is therefore interpreted to be younger than the ~19 Ma phase of this intrusion (Harrison et al., 1999).

The Lower and Upper Levels and the overlying Tethyan sedimentary sequence form a cohesive structural block after movement along the Phu detachment ceased sometime after ~19 Ma (Fig. 10(D)). The cohesive block of the Lower and Upper Levels and the overlying Tethyan sedimentary sequence is folded by crustal-scale open folds. The Mutsog synform and Chako antiform are a non-cylindrical antiform- synform pair, recording this younger contraction. Secondary magnetic remanences of samples from the north limb of the Chako antiform also record a late clockwise rotation mimicking the rotation of the fold limb of these folds (Schill et al., 2003).

The Mutsog synform and Chako antiform complicate the geometry of the Marsyandi valley-Manaslu area in three ways: they modify the homoclinal geometry of the Greater Himalayan sequence in the Marsyandi and Nar valleys; they produce an apparent (Chako) dome (Bordet et al., 1975); and finally, they generate apparent orogen perpendicular movement along the Chame detachment by folding part of the Chame detachment into a orogen-parallel orientation after it ceased movement (Coleman, 1996).

6.6. At ~14 Ma (?)

Zones of steep north–south meso-scale brittle faults and fractures are the youngest structural feature (D_4) preserved in the Nar valley. The north–south drainage of the Nar valley, and the ~3500 m-high vertical east face of Chubche are similar in orientation to D_4 features. D_4 small-scale brittle faults cross-cut D_{2L} features and are thus younger than D_{2L} (~20 Ma). The Nar valley drainage and the east face of Chubche cross-cut D_3 megascopic folds, suggesting D_4 is younger than D_3 (<19 Ma).

The late, D_4 brittle faults are geometrically similar to N–S steeply-dipping brittle faults observed in the Marsyandi valley and in the neighbouring Kali Gandaki valley (Coleman and Hodges, 1995; Godin, 2003). Coleman and Hodges (1995) dated hydrothermal muscovite grown synkinematic to late, north–south brittle faulting. A plateau age of 14.3 ± 0.9 Ma was derived using ^{40}Ar–^{39}Ar thermochronology, and interpreted to indicate activity in the Thakkhola graben structure and marking the development of E–W extension of the southern Tibetan Plateau (Coleman and Hodges, 1995).

7. Conclusions

The Greater Himalayan sequence in the study area is composed of structurally differentiable Lower and Upper Levels. The Upper Level, originally considered to be part of the Tethyan sedimentary sequence, is interpreted as part of the Greater Himalayan sequence based on high-grade metamorphic assemblages and 500–650 °C peak metamorphic temperatures. This geographically expands the metamorphic core and refines Himalayan nomenclature, by adding two units (units IV and V), to the well-known units I, II, and III of the Greater Himalayan sequence in the Annapurna region.

Differences in structural style suggest the Lower and Upper Levels may have different early tectonometamorphic histories. The two levels were juxtaposed along the synmetamorphic Chame detachment ca. 20 Ma during retrograde metamorphism. Interpreting the Chame detachment as wholly within the Greater Himalayan sequence reconciles previously contradictory interpretations of a metamorphic dome in the immediate hanging wall of a detachment fault. After ~19 Ma, the Phu detachment placed the unmetamorphosed Tethyan sedimentary sequence onto the Upper Level. The Lower and Upper Levels and the Tethyan sedimentary sequence were folded, after 19 Ma, by a non-cylindrical antiform-synform pair with a ~25 km wavelength which created an apparent dome.

Metamorphic domes previously thought to be protruding through Tethyan sedimentary sequence, like the Chako Dome, may actually be folded sections of metamorphic rock, in turn affecting the overlying lower grade metamorphic and sedimentary carapace. Our study also indicates that large amplitude post-metamorphic crustal-scale folding has significantly modified the present-day architecture of the extruding slab.

Acknowledgements

This research was supported by the Natural Science and Engineering Research Council of Canada Discovery Grant and scholarship to L.G. and T.G., respectively. Financial support from the Department of Earth Sciences at Simon Fraser University is also acknowledged. Dan Marshall is thanked for his insight into metamorphic petrology. We wish to thank Pasang Tamang and his team for invaluable field support, and Charlotte Olson for excellent assistance in the field. Earlier versions of this paper benefited from constructive reviews by Stéphane Guillot, An Yin, Mike Edwards, Mike Searle, and Journal Editor Kevin Burke.

Appendix. Thermometry method

Three unit V samples (Fig. 4) were analysed on the Cameca SX-50 microprobe at the University of British Columbia. Two

samples consisted of garnet-biotite schist (T-105 & N-102) and the other was garnet-biotite phyllite (N-38). Samples T-105 and N-102 are from adjacent stations at the same structural level. Sample N-38 is ~500 m structurally higher and 14 km north of T-105 and N-102. For each sample, multiple garnets were traversed with perpendicular traverses. Biotite inclusions in garnet, biotite adjacent to garnet and matrix biotite were analysed for each traversed garnet.

Core temperatures are calculated by pairing biotite inclusions in a garnet porphyroblast with a nearby garnet core point. Rim temperatures are calculated by pairing an adjacent biotite to a rim garnet point (Hodges and Crowley, 1985). Temperatures of representative samples were calculated by Gleeson (2003) manually following the method of Ferry and Spear (1978). Additional representative pairs were analysed using TWEEQU (Berman, 1991). TWEEQU uses the Berman (1990) garnet activity model and the McMullin et al. (1991) biotite activity model. Temperature ranges from TWEEQU graphs were derived using 9 kbar as a reasonable prograde and peak metamorphic pressure for central Nepal (Vannay and Hodges, 1996; Guillot et al., 1999).

References

Arita, K., 1983. Origin of the inverted metamorphism of the lower Himalayas, central Nepal. Tectonophysics 95, 43–60.

Beaumont, C., Jamieson, R.A., Nguyen, M.H., Lee, B., 2001. Himalayan tectonics explained by extrusion of a low-viscosity crustal channel coupled to focused surface denudation. Nature 414, 738–742.

Berman, R.G., 1990. Mixing properties of Ca–Mg–Fe–Mn garnets. American Mineralogist 75, 328–344.

Berman, G., 1991. Thermobarometry using multiequilibrium calculations: a new technique, with petrological applications. Canadian Mineralogist 29, 833–855.

Bordet, P., Colchen, M., Le Fort, P., 1975. Recherches géologiques dans l'Himalaya du Népal: région du Nyi-Shang, Éditions du Centre National de la Recherche Scientifique: Paris, France, Centre National de la Recherche Scientifique, 138 p.

Bouchez, J.L., Pêcher, A., 1981. The Himalayan main central thrust pile and its quartz-rich tectonites in central Nepal. Tectonophysics 78, 23–50.

Brown, R.L., and, Nazarchuk, J.H., 1993. Annapurna detachment fault in the Greater Himalaya of central Nepal. In: Treloar, P.J., Searle, M.P. (Eds.), Himalayan Tectonics, Geological Society Special Publication, 74, pp. 461–473.

Brunel, M., 1986. Ductile thrusting in the Himalayas: shear sense criteria and stretching lineations. Tectonics 5, 247–265.

Brunel, M., Kienast, J.-R., 1986. étude pétro-structurale des chevauchements ductiles himalayens sur la traversale de l'Everest-Makalu (Népal oriental). Canadian Journal of Earth Sciences 23, 1117–1137.

Burchfiel, B.C., Royden, L.H., 1985. North–south extension within the convergent Himalayan region. Geology 13, 679–682.

Burchfiel, B.C., Chen, Z., Hodges, K.V., Liu, Y., Royden, L.H., Deng, C., Xu, J., 1992. The South Tibetan Detachment System, Himalaya Orogen: Extension contemporaneous with and parallel to shortening in a collisional mountain belt, Geological Society of America Special Paper 269, p. 41.

Burg, J.-P., Guirand, M., Chen, G.M., Li, G.C., 1984. Himalayan metamorphism and deformations in the North Himalayan Belt (Southern Tibet China). Earth and Planetary Science Letters 69, 391–400.

Caby, R., Pêcher, A., Le Fort, P., 1983. Le Grand chevauchement central himalayen: nouvelles données sur le métamorphisme inverse à la base de la Dalle du Tibet. Revue de Géologie Dynamique et Géographie Physique 24, 89–100.

Colchen, M., Le Fort, P., Pêcher, A., 1981. In: Gupta, H.K., Delany, F.M. (Eds.), Geological map of Annapurnas–Manaslu–Ganesh Himalaya of Nepal. Zagros-Hindu Kush-Himalaya geodynamic evolution, Washington, DC (American Geophysical Union, scale 1:200,000).

Colchen, M., Le Fort, P., Pêcher, A., 1986. Annapurna–Manaslu–Ganesh Himal, Recherches geologiques dans L'Himalaya du Nepal. Centre National de la Recherche Scientifique, Paris p. 136.

Coleman, M.E., 1996. Orogen-parallel and orogen-perpendicular extension in the central Nepalese Himalayas. Geological Society of America Bulletin 108, 1594–1607.

Coleman, M.E., 1998. U-Pb constraints on Oligocene–Miocene deformation and anatexis within the central Himalaya, Marsyandi valley, Nepal. American Journal of Science 298, 553–571.

Coleman, M., Hodges, K.V., 1995. Evidence for Tibetan plateau uplift before 14 Myr ago from a new minimum age for east-west extension. Nature 374, 49–52.

Coleman, M.E., Hodges, K.V., 1998. Contrasting Oligocene and Miocene thermal histories from the hanging wall and footwall of the South Tibetan detachment in the central Himalaya from $^{40}Ar/^{39}Ar$ thermochronology, Marsyandi valley, central Nepal. Tectonics 17, 726–740.

Davis, G.H., Reynolds, S.J., 1996. Structural geology of rocks and regions. Wiley, New York p. 776.

Ferry, J.M., Spear, F.S., 1978. Experimental calibration for the partitioning of Fe and Mg between biotite and garnet. Contributions to Mineralogy and Petrology 66, 113–117.

Fuchs, G., Widder, R.W., Tuladhar, R., 1988. Contributions to the geology of the Annapurna range (Manang, area, Nepal). Jahrbuch der Geologischen Bundesanstalt, Wien 131, 593–607.

Gaetani, M., Garzanti, E., 1991. Multicyclic history of the Northern India continental margin (Northwestern Himalaya). American Association of Petroleum Geologists Bulletin 75, 1427–1446.

Gansser, A., 1964. Geology of the Himalayas: London. Wiley, New York p. 289.

Garzanti, E., 1999. Stratigraphy and sedimentary history of the Nepal Tethys Himalaya passive margin. Journal of Asian Earth Sciences 17, 805–827.

Garzanti, E., Gorza, M., Martellini, L., Nicora, A., 1994. Transition from diagenesis to metamorphism in the Paleozoic to Mesozoic succession of the Dolpo-Manang Synclinorium and Thakkhola graben (Nepal Tethys Himalaya). Eclogae Geologicae Helvetica 87, 613–632.

Gehrels, G.E., DeCelles, P.G., Martin, A., Ojha, T., Pinhassi, G., 2003. Initiation of the Himalayan orogen as an Early Paleozoic thin-skinned thrust belt. Geological Society of America Today, September, 4–9.

Gleeson, T.P., 2003. Tectonometamorphic evolution of the lower Nar Valley, Central Nepal Himlaya [Unpublished MSc thesis]: Simon Fraser University, p. 99.

Godin, L., 2001. The Chako dome: an enigmatic structure in the hanging wall of the South Tibetan detachment, Nar valley, central Nepal. Journal of Asian Earth Sciences 19, 22–23.

Godin, L., 2003. Structural evolution of the Tethyan sedimentary sequence, central Nepal Himalaya. Journal of Asian Earth Sciences 22, 307–328.

Godin, L., Brown, R.L., Hanmer, S., 1999a. High strain zone in the hanging wall of the Annapurna detachment, central Nepal Himalaya. In: Macfarlane, A.M., Sorkhabi, R., Quade, J. (Eds.), Himalaya and Tibet: Mountain roots to mountain tops Geological Society of America Special Paper, 328, pp. 199–210.

Godin, L., Brown, R.L., Hanmer, S., Parrish, R., 1999b. Backfolds in the core of the Himalayan orogen: an alternative interpretation. Geology 27, 151–154.

Godin, L., Parrish, R.R., Brown, R.L., Hodges, K., 2001. Crustal thickening leading to exhumation of the metamorphic core of the central Nepal Himalaya: insight from U-Pb geochronology and $^{40}Ar/^{39}Ar$ thermochronology. Tectonics 20, 729–747.

Godin, L., Glesson, T., Searle, M.P., Ullrich, T.D. and Parrish, R.R., in press. Locking of southward extrusion in favor of rapid crustal-scale buckling of the Greater Himalayan sequence, Nor valley, central Nepal. In "Channel Flow, Ductile extrusion and exhumation in continental collision zones". R.D. Law, M.P. Searle and L. Godin (eds.), Geological Soceity, London, Special Publication.

Gradstein, F.M., von Rad, U., Gibling, M.R., Jansa, L.F., Kaminski, M.A., Kristiansen, I.-L., Ogg, J.G., Rohl, U., Sarti, M., Thorow, J.W., Westermann, G.E.G., Wiedmann, J., 1992. The Mesozoic continental margin of central Nepal. Geologisches Jahrbuch 77.

Grasemann, B., Fritz, H., Vannay, J.-C., 1999. Quantitative kinematic flow analysis from the Main Central thrust zone (NW-Himalaya India): implications for a decelerating strain path and the extrusion of orogenic wedges. Journal of Structural Geology 21, 837–853.

Grujic, D., Casey, M., Davidson, C., Hollister, L.S., Kündic, R., Pavlis, T., Schmid, S., 1996. Ductile extension of the Higher Himalayan Crystalline in Bhutan: evidence from quartz microfabrics. Tectonophysics 260, 21–43.

Grujic, D., Hollister, L.S., Parrish, R., 2002. Himalayan metamorphic sequence as an orogenic channel: insights from Bhutan. Earth and Planetary Science Letters 198, 177–191.

Guillot, S., Pêcher, A., Rochette, P., Le Fort, P., 1993. The emplacement of the Manaslu granite of Central Nepal: field and and magnetic susceptibility constraints. In: Treolar, P.J., Searle, M. (Eds.), Himalayan Tectonics Geological Society Special Publication, 74, pp. 413–428.

Guillot, S., Hodges, K.V., Le Fort, P., Pêcher, A., 1994. New constraints on the age of the Manaslu leucogranite: evidence for episodic tectonic denudation in the central Himalayas. Geology 22, 559–562.

Guillot, S., Cosca, M., Allemand, P., Le Fort, P., 1999. Contrasting metamorphic and geochronologic evolution along the Himalayan belt. In: Macfarlane, A.M., Sorkhabi, R., Quade, J. (Eds.), Himalaya and Tibet: Mountain roots to mountain tops Geological Society of America Special Paper, 328, pp. 117–128.

Hanmer, S., 1984. Strain insensitive foliations in polymineralic rocks. Canadian Journal of Earth Sciences 21, 1410–1414.

Harrison, T.M., Grove, M., McKeegan, K.D., Coath, C.D., Lovera, O.M., Le Fort, P., 1999. Origin and episodic emplacement of the Manaslu intrusive complex, central Himalaya. Journal of Petrology 40, 3–19.

Hodges, K.V., 2000. Tectonics of the Himalaya and southern Tibet from two perspectives. Geological Society of America Bulletin 112, 324–350.

Hodges, K.V., Crowley, P.D., 1985. Error estimation and empirical geothermobarometry for peletic systems. American Mineralogist 70, 702–709.

Hodges, K.V., Hubbard, M.S., Silverberg, D.S., 1988. Metamorphic constraints on the thermal evolution of the central Himalayan orogen. Philosophical Transactions of the Royal Society of London A326, 257–280.

Hodges, K.V., Parrish, R.R., Searle, M.P., 1996. Tectonic evolution of the central Annapurna range, Nepalese Himalayas. Tectonics 15, 1264–1291.

Hubbard, M.S., 1996. Ductile shear as a cause of inverted metamorphism: example from the Nepal Himalaya. Journal of Geology 104, 493–499.

Hubbard, M.S., Harrison, T.M., 1989. $^{40}Ar/^{39}Ar$ age constraints on deformation and metamorphism in the Main Central Thrust Zone and Tibetan Slab, eastern Nepal Himalaya. Tectonics 8, 865–880.

Inger, S., Harris, N., 1992. Tectonothermal evolution of the High Himalayan crystalline sequence, Langtang valley, Northern Nepal. Journal of Metamorphic Geology 10, 439–452.

Kretz, R., 1983. Symbols for rock-forming minerals. American Mineralogist 68, 277–279.

Law, R.D., Searle, M.P., Simpson, R.L., 2004. Strain, deformation temperatures and vorticity of flow at the top of the Greater Himalayan slab, Everest massif, Tibet. Journal of Geological Society of London 161, 305–320.

Le Fort, P., 1975. Himalayas: the collided range. Present knowledge of the continental arc. American Journal of Science 275, 1–44.

Le Fort, P., Guillot, S., 1998. Preliminary results of Himlung expedition to northern Manaslu massif, central Nepal. Special Issue, Geological Bulletin of Peshwar 31, 110–113.

Le Fort, P., Cuney, C., Deniel, C., France-Lanord, C., Shepard, S.M.F., Upreti, B.N., Vidal, P., 1987. Crustal generation of the Himalayan leucogranites. Tectonophysics 134, 39–57.

Le Fort, P., Guillot, S., Pêcher, A., 1999. Une carte géologique de l'Himlung Himal, massif du Manaslu, La Montagne Alpinisme, Club alpin francais, Paris, p. 22–27

McMullin, D., Berman, R.G., Greenwood, H.J., 1991. Calibration of the SGAM thermobarometer for pelitic rocks using data from phase equilibrium experiments and natural assemblages. Canadian Mineralogist 29, 889–908.

Molnar, P., England, P., Martinod, J., 1993. Mantle dynamics, uplift of the Tibetan Plateau, and the Indian monsoon. Reviews in Geophysics 31, 357–396.

Nazarchuk, J.H., 1993. Structure and geochronology of the Greater Himalaya, Kali Gandaki region, West-Central Nepal [Unpublished MSc thesis thesis]: Carleton University.

Nelson, K.D., Zhao, W., Brown, L.D., Kuo, J., Che, J., Liu, X., Lemperer, S.L., Makolsky, Y., Meissner, R., Mechie, J., Kind, R., Wenzel, F., Ni, J., Nablek, J., Leshou, C., Tan, H., Wei, W., Jones, A.G., Booker, J., Unsworth, M., Kidd, W.S.F., Hauck, M., Alsdorf, D., Ross, A., Cogan, M., Wu, C., Sandvol, E., Edwards, M., 1996. Partially molten middle crust beneath southern tibet: synthesis of project INDEPTH Results. Science 274, 1684–1688.

Passchier, C.W., Trouw, R.A.J., 1998. Microtectonics. Springer, Berlin p. 289.

Pêcher, A., 1975. The Main Central Thrust of the Nepal Himalaya and the related metamorphism in the Modi-Khola cross-section (Annapurna Range). Himalayan Geology 5, 115–132.

Pêcher, A., 1989. The metamorphism in Central Himalaya. Journal of Metamorphic Geology 7, 31–41.

Pêcher, A., Le Fort, P., 1986. The metamorphism in Central Himalaya, its relations with the thrust tectonic. In: Le Fort, P., Colchen, M., Montenat, C. (Eds.), Evolution des domaines orogéniques d'Asie méridionale (de la Turquie à l'Indon_ésie) Science de la Terre, Nancy, 47 p. 285–309.

Reddy, S.M., Searle, M.P., Massey, J.A., 1993. Structural evolution of the high Himalayan gneiss sequence, Langtang valley, Nepal. In: Treloar, P.J., Searle, M.P. (Eds.), Himalayan Tectonics Geological Society Special Publication, 74, pp. 375–389.

Royden, L.H., Burchfiel, B.C., King, R.W., Wang, E., Liu, E., Chen, Z.F., Shen, F., Liu, Y., 1997. Surface deformation and lower crustal flow in eastern Tibet. Science 276, 788–790.

Schill, E., Appel, E., Godin, L., Crouzet, C., Gautam, P., Regmi, K.R., 2003. Record of deformation by secondary magnetic remanances and magnetic anistropy in the Nar/Phu valley (central Himalaya). Tectonophysics 377, 197–209.

Schneider, C., Masch, L., 1993. The metamorphism of the Tibetan Series from the Manang area, Marsyandi valley, central Nepal. In: Treloar, P.J., Searle, M.P. (Eds.), Himalayan Tectonics Geological Society Special Publication, 74, pp. 357–374.

Searle, M.P., 1999. Extensional and compressional faults in the Everest-Lhotse massif, Khumbu Himalaya, Nepal. Journal of the Geological Society of London 156, 27–240.

Searle, M.P., Godin, L., 2003. The South Tibetan detachment system and the Manaslu leucogranite: a structural re-interpretation and restoration of the Annapurna–Manaslu Himalaya, Nepal. Journal of Geology 111, 505–523.

Searle, M.P., Windley, B.F., Coward, M.P., Cooper, D.J.W., Rex, A.J., Rex, D., Tingdong, L., Xuchang, X., Jan, M.Q., Thakur, V.C., Kumar, S., 1987. The closing of Tethys and the tectonics of the Himalaya. Geological Society of America Bulletin 98, 678–701.

Searle, M.P., Parrish, R.R., Hodges, K.V., Hurford, A., Ayres, M.W., Whitehouse, M.J., 1997. Shisha Pangma leucogranite, South Tibet: Field relations, geochemistry, age, origin and emplacement. Journal of Geology 105, 295–317.

Searle, M.P., Simpson, R.L., Law, R.D., Parrish, R., Waters, D.J., 2003. The structural geometry, metamorphic and magmatic evolution of the Everest massif, high Himalaya of Nepal-South Tibet. Journal of the Geological Society, London 160, 345–366.

Vannay, J.-C., Hodges, K.V., 1996. Tectonometamorphic evolution of the Himalayan metamorphic core between the Annapurna and Dhaulagiri, central Nepal. Journal of Metamorphic Geology 14, 635–656.

Vannay, J.-C., Grasemann, B., 2001. Himalayan inverted metamorphism and syn-convergence extension as a consequence of a general shear extrusion. Geological Magazine 138, 253–276.

Weismayr, G., Grasemann, B., 2002. Eohimalayan fold and thrust belt: Implications for the geodynamic evolution of the NW-Himalaya (India). Tectonics 21, 8-1–8-18.

Yardley, B.W., 1991. An introduction to metamorphic petrology: Essex, Longman Scientific and Technical, 272 p.

Yin, A., Harrison, T.M., 2000. Geologic evolution of the Himalayan-Tibetan orogen. Annual Reviews in Earth and Planetary Science 28, 211–280.